nature cell biology

Inter-organ signalling by HRG-7 promotes systemic haem homeostasis

Jason Sinclair[1], Katherine Pinter[1], Tamika Samuel[1], Simon Beardsley[1], Xiaojing Yuan[1], Jianbing Zhang[1], Kevin Meng[1], Sijung Yun[2], Michael Krause[2] and Iqbal Hamza[1,3]

Growing evidence in vertebrates predicts that cellular haem levels in animals are maintained not only by a cell's internal capacity for haem synthesis in a cell-autonomous manner, but also by an inter-organ haem trafficking network through cell-non-autonomous regulation. Using *Caenorhabditis elegans*, a genetically and optically amenable animal model for visualizing haem-dependent signalling, we show that HRG-7, a protein with homology to aspartic proteases, mediates inter-organ signalling between the intestine and extra-intestinal tissues. Intestinal HRG-7 functions as a secreted signalling factor during haem starvation in extra-intestinal tissues and is regulated through a DBL-1, homologous to BMP5, dependent signal from neurons. Given the evidence that vertebrate homologues exist for each of the components of the HRG-7-mediated signalling pathway, it is conceivable that the cell-non-autonomous signalling framework that we uncovered in *C. elegans* may have functional relevance for inter-organ regulation of iron and haem metabolism in humans.

Haem is an iron-containing porphyrin that is required as a prosthetic group in a variety of proteins crucial for cellular functions including globins for gas-binding, cytochromes for electron transfer, and guanylate cyclase for cellular signalling[1,2]. It is generally accepted that cellular requirements for haem in animals are fulfilled by the cell's internal capacity to regulate and synthesize its own haem, that is, cell-autonomous regulation[3]. However, several lines of evidence in humans, mice and zebrafish support the existence of a cell-non-autonomous regulation by a systemic haem communication system even though they are capable of intracellular haem synthesis[4–8].

Caenorhabditis elegans is ideal to determine whether such systemic signalling pathways exist as it overcomes several obstacles encountered in mammalian models[9]. Worms are haem auxotrophs permitting external control of intracellular haem levels, can be manipulated and observed live at subcellular resolution, and are optically transparent for *in vivo* monitoring of haem signals between tissues during development[9,10]. Herein, we show that HRG-7 mediates cell-non-autonomous haem signalling by functioning as a secreted factor and communicating intestinal haem status with extra-intestinal tissues. Reciprocally, a DBL-1-dependent signal from the neurons transcriptionally regulates both *hrg-7* and intestinal haem transport. Our work provides a cell biological model for how organs communicate their haem status to regulate metabolism at the organismal level[11].

RESULTS

A genome-wide RNAi screen identifies HRG-7 as a regulator of systemic haem homeostasis

Our previous studies revealed that *C. elegans* imports haem into the intestine by the concerted functions of HRG-4 on the plasma membrane and HRG-1 on endo-lysosomal membranes, which mobilizes haem from vesicles, while the ABCC-type transporter MRP-5 is the major intestinal haem exporter. Loss of *hrg-4* results in reduced haem transport into the intestine, whereas loss of *mrp-5* causes haem accumulation within the intestine while extra-intestinal tissues become haem-deprived[8,12]. Depletion of either gene results in robust upregulation of GFP in the transgenic *C. elegans* haem sensor strain IQ6011 ($P_{hrg\text{-}1}$::*GFP*), which shows strong GFP expression under low haem conditions (Fig. 1a). While this result is expected for depletion of *hrg-4*, it is paradoxical for *mrp-5* depletion as intestinal haem accumulation should normally suppress this GFP reporter[12–14]. One potential explanation for GFP reporter upregulation is that the haem sensor strain responds not only to intestinal haem deficiency, as in the case of *hrg-4* depletion, but also to haem starvation signals emanating from the extra-intestinal tissues due to *mrp-5* deficiency[8], a concept originally proposed to exist for the regulation of inter-tissue copper and iron homeostasis in mammals[15–17].

To identify factors involved in inter-tissue haem homeostasis, we exploited the $P_{hrg\text{-}1}$::*GFP* haem sensor worms to perform a

[1]Department of Animal & Avian Sciences and Department of Cell Biology & Molecular Genetics, University of Maryland, College Park, Maryland 20742, USA.
[2]Laboratory of Molecular Biology, National Institute of Diabetes and Digestive and Kidney Diseases, National Institutes of Health, Bethesda, Maryland 20892, USA.
[3]Correspondence should be addressed to I.H. (e-mail: hamza@umd.edu)

Received 30 August 2016; accepted 27 April 2017; published online 5 June 2017; DOI: 10.1038/ncb3539

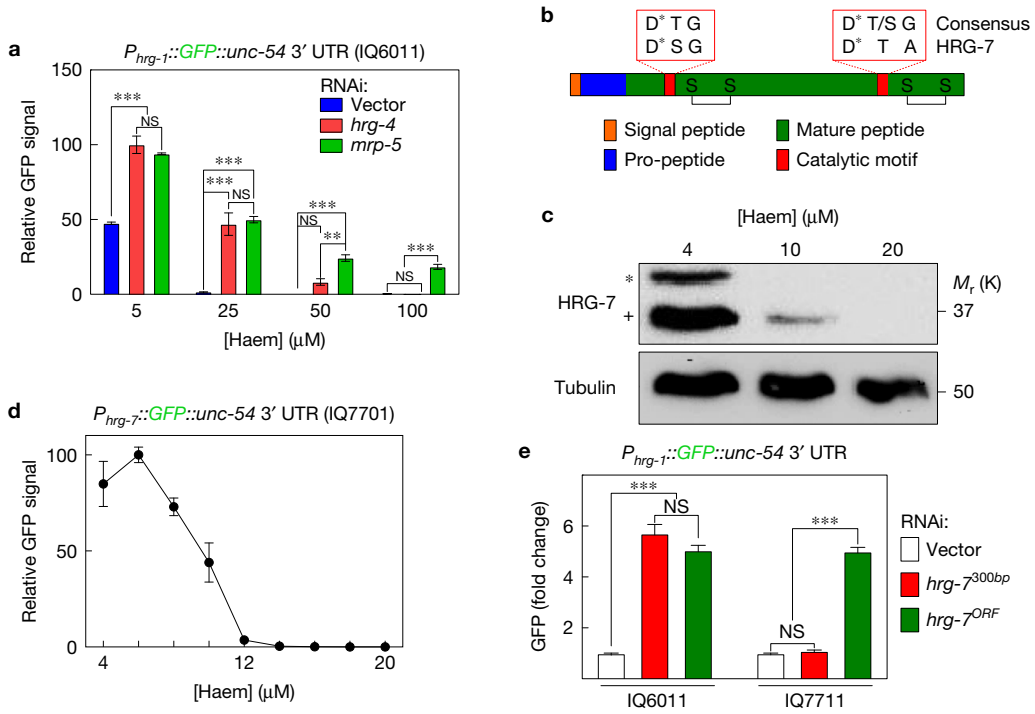

Figure 1 Haem homeostasis is regulated by the aspartic protease homologue *hrg-7*. (**a**) GFP fluorescence quantified from strain IQ6011 ($P_{hrg\text{-}1}$::*GFP*) fed dsRNA against control vector, *hrg-4* or *mrp-5* at 5, 25, 50 and 100 μM haem. GFP was quantified using COPAS BioSort. GFP is represented as fold change compared with vector. The graph represents the mean and s.e.m. of three biologically independent experiments. $n=120$ worms per treatment per experiment. $^{***}P<0.001$, $^{**}P<0.01$ (two-way ANOVA). NS, not significant. See Supplementary Table 3 for statistics source data. (**b**) Cartoon depicting general features of aspartic proteases. * indicates catalytic Asp residues. (**c**) Immunoblot analysis of HRG-7 expression in N2 grown in increasing haem concentrations. Membranes were probed with polyclonal anti-HRG-7 antibody and then incubated with HRP-conjugated anti-rabbit secondary antibody. * indicates pro-HRG-7. + indicates mature HRG-7. Unprocessed original scans of blots are shown in Supplementary Fig. 6. Data are representative of three independent experiments. (**d**) GFP expression in strain IQ7701 ($P_{hrg\text{-}7}$::*GFP*) grown in varying haem concentrations. GFP was quantified with the COPAS BioSort. GFP is represented as relative intensity on a scale of 1–100. The graph represents the mean and s.e.m. of three biologically independent experiments. $n=100$ worms per treatment per experiment. (**e**) GFP fluorescence quantified from IQ6011 ($P_{hrg\text{-}1}$::*GFP*) and IQ7711 ($P_{vha\text{-}6}$::*HRG-7*^{PR}::*ICS*::*mCherry*; $P_{hrg\text{-}1}$::*GFP*) fed dsRNA against control vector, *hrg-7*^{300bp} and *hrg-7*^{ORF} at 10 μM haem. GFP was quantified using COPAS BioSort. GFP is presented as fold change compared with vector. The graph represents the mean and s.e.m. of three biologically independent experiments. $n=120$ worms per treatment per experiment. $^{***}P<0.001$ (one-way ANOVA). NS, not significant. See Supplementary Table 3 for statistics source data.

feeding RNA-mediated interference (RNAi) screen by systematically depleting 18,533 genes that encompass ~93% of the worm genome. To eliminate genes that regulated GFP non-specifically, we rescreened 1,641 positive hits in the $P_{vha\text{-}6}$::*GFP* worms, which express intestinal GFP independent of haem. GFP was quantified using COPAS BioSort flow cytometry; genes were considered candidates if knockdown resulted in regulation of $P_{hrg\text{-}1}$::*GFP* by ≥2 fold (log scale) compared with $P_{vha\text{-}6}$::*GFP*; we found 177 genes that preferentially regulated $P_{hrg\text{-}1}$::*GFP* (Supplementary Table 4). A comparison of these candidate genes with the 288 haem-responsive genes that we had previously identified from microarray experiments[14] revealed three overlapping genes between the two data sets: *mrp-5*, *R193.2* and *C15C8.3*. Both *mrp-5* and *R193.2* encode multiple transmembrane domain-containing proteins while *C15C8.3* encodes a soluble protein containing a signal peptide, an indication that the protein could potentially be secreted and thus capable of cell–cell communication. We termed *C15C8.3* as *haem-responsive gene 7* (*hrg-7*).

HRG-7 is a putative member of the A1 family of aspartic proteases. Like other members of this family, HRG-7 contains a predicted signal peptide, a pro-region that is cleaved during protein maturation, conserved cysteines for disulfide bonds, and an active site containing aspartic acids essential for proteolytic cleavage (Fig. 1b). Antibodies generated against the carboxy-terminal 17 amino acid residues of HRG-7 detected two forms of HRG-7 (corresponding to the pro and mature forms of the predicted proteins) on immunoblots of lysates from worms grown in low haem but not in 20 μM haem (Fig. 1c). Consistent with the effect of haem on HRG-7, genomic sequence alignment of *hrg-7* from three *Caenorhabditis* species (*C. elegans*, *C. briggsae* and *C. remanei*) revealed a conserved *cis*-regulatory element termed haem responsive element (HERE) in the 5′ upstream region (Supplementary Fig. 1a)[18]. The *hrg-7* HERE, as previously demonstrated for the *hrg-1* promoter, is flanked by GATA elements that are responsible for intestinal gene expression in *C. elegans*[19]. Indeed, transgenic worms bearing the $P_{hrg\text{-}7}$::*GFP* transcriptional reporter (strain IQ7701) showed strong GFP expression in the intestine only under low haem conditions that was suppressed either by haem in a dose-dependent manner (Fig. 1d and Supplementary Fig. 1b) or by mutagenesis of the HERE (Supplementary Fig. 1c).

To determine whether HRG-7 regulates intestinal haem homeostasis, we expressed an RNAi-resistant form of *hrg-7* (*hrg-7*^{PR}) from

the intestinal-specific *vha-6* promoter in the $P_{hrg\text{-}1}$*::GFP* haem sensor worms. The *hrg-7*^{PR} transgene contains a recoded portion within its open-reading frame (ORF) such that it is resistant to double-stranded RNA (dsRNA) directed against the first 300 base pairs (*hrg-7*^{300bp}), but it is susceptible to dsRNA directed against the remainder of the ORF (*hrg-7*^{ORF}) (Supplementary Fig. 1d,e). Thus, *hrg-7*^{PR} expression permits interrogation of transgene function in the presence or absence of endogenous *hrg-7*. Intestinally expressed *hrg-7*^{PR} restored $P_{hrg\text{-}1}$*::GFP* expression to wild-type (WT) levels when *hrg-7* was depleted by *hrg-7*^{300bp}, but not with *hrg-7*^{ORF} (Fig. 1e). These results show that HRG-7 is required to maintain intestinal haem homeostasis under low haem conditions.

HRG-7 is secreted from the intestine for cell-non-autonomous regulation of intestinal haem homeostasis

Because *hrg-7* depletion in the $P_{hrg\text{-}1}$*::GFP* haem sensor worms resulted in a haem deficiency readout even in the presence of excess haem, we examined whether intestinal haem uptake was aberrant when *hrg-7* is depleted. RNAi depletion of haem importers, *hrg-1* and *hrg-4*, resulted in the expected alteration in accumulation of the fluorescent haem analogue zinc mesoporphyrin (ZnMP), while *hrg-7* knockdown showed no effect on the ZnMP signal (Supplementary Fig. 2a)[13]. We next examined HRG-7 protein localization in transgenic worms expressing a $P_{hrg\text{-}7}$*::HRG-7::mCherry* translational reporter. Unexpectedly, little or no signal was detected for HRG-7::mCherry within the intestine of worms grown in low haem. Instead, HRG-7::mCherry localized to distinct punctate structures near the anterior and posterior regions of the worm (Fig. 2a). HRG-7::mCherry also accumulated within coelomocytes, macrophage-like cells that take up proteins and compounds from the body cavity, an attribute that is typically exploited as a marker for secretion into the pseudocoelom (Fig. 2a)[20]. This unexpected localization was not due to ectopic expression of the *hrg-7* transgene as HRG-7 accumulated in similar extra-intestinal structures when directed from the intestinal-specific *vha-6* promoter (Supplementary Fig. 2b,c)[21,22]. Co-expression with the coelomocyte marker $P_{unc\text{-}122}$*::GFP* verified HRG-7::mCherry secretion (Supplementary Fig. 2c). Although fluorescent-tagged secreted proteins could accumulate nonspecifically in coelomocytes, the distinct punctate localization of HRG-7::mCherry was highly specific as there was no overlap with either full-length or signal peptide HRG-3::mCherry, another secreted protein that delivers intestinal haem to extra-intestinal tissues (Supplementary Fig. 2d)[23].

To identify the tissue location of secreted HRG-7, we generated double transgenic worms co-expressing $P_{vha\text{-}6}$*::HRG-7::mCherry* plus a marker for either body wall muscle, hypodermis, pharyngeal muscle, or neurons (Fig. 2b and Supplementary Fig. 2e). HRG-7::mCherry co-localized strongly with only the pan-neuronal GFP marker ($P_{unc\text{-}119}$*::GFP*) (Fig. 2b). Reconstruction of 0.5-µm-thick confocal sections revealed that secreted HRG-7::mCherry was located within puncta in a bundle of head neurons near the nerve ring. In *C. elegans*, chemosensory neurons appear to have a critical role in nutrient homeostasis and project cilia to the external medium permitting detection by uptake of 5-fluorescein isothiocyanate (FITC) dye[24–26]. HRG-7::mCherry co-localized with these FITC-positive neurons in both the anterior (amphids) and posterior (phasmids) of the worm, indicating that HRG-7 preferentially localizes to sensory neurons (Fig. 2c). To corroborate HRG-7 localization, we generated $P_{vha\text{-}6}$*::HRG-7-3xFLAG::ICS::GFP*. In this strain, *gfp* and *hrg-7-3xFLAG* are initially transcribed as a single polycistronic pre-messenger RNA but the intercistronic (ICS) sequence is SL2 trans-spliced generating two mRNAs that are translated independently, making this transgenic construct ideal for separating mRNA expression from protein localization[27]. Immunohistochemistry with a commercial monoclonal FLAG antibody detected HRG-7::3xFLAG in both the intestine and neurons, but the GFP fluorescence was limited to the intestine as expected (Fig. 2d). These results further confirm that HRG-7 is synthesized in the intestine but is secreted and localizes to neuronal structures.

To determine whether intestinally produced HRG-7 functions intracellularly (autonomous) or extracellularly (non-autonomous), we tethered HRG-7::mCherry to intestinal cells by mutating the signal peptidase cleavage site (TM-HRG-7), as retention of the signal peptide should act as a transmembrane anchor. Predictably, TM-HRG-7 was not secreted, but rather retained within the worm intestine (Fig. 2e). We then evaluated whether TM-HRG-7 was capable of suppressing the haem deficiency signal in haem sensor worms by using RNAi-resistant transgenes. The $P_{hrg\text{-}1}$*::GFP* sensor was significantly repressed only when HRG-7::mCherry was secreted but not when it was tethered to intestinal cells, implying that HRG-7 functions extracellularly to regulate intestinal haem responsiveness (Fig. 2f).

We next determined the source of the haem deficiency signal in *hrg-7* mutant worms by depleting *hrg-7* in combination with either the haem importer *hrg-4* or the haem exporter *mrp-5* in the $P_{hrg\text{-}1}$*::GFP* haem sensor strain. Co-RNAi knockdown of either *hrg-4* and *hrg-7* or *hrg-4* and *mrp-5* resulted in an enhanced haem deficiency signal phenotype that was not observed when *hrg-7* and *mrp-5* were co-depleted (Supplementary Fig. 2f). Because *mrp-5* depletion causes extra-intestinal haem deficiency secondary to intestinal haem overload, we infer that the lack of a synergistic effect in *hrg-7* and *mrp-5* double RNAi worms is due to both genes regulating intestinal haem responsiveness by altering extra-intestinal haem homeostasis.

Functionally mature HRG-7 is produced solely by the intestine

To evaluate HRG-7 secretion, we expressed HRG-7::mCherry from the inducible *hsp-16.2* promoter. The *hsp-16.2* promoter is activated in several tissues, including the intestine, following a transient exposure of worms to 37 °C (ref. 28). Approximately 180 min following heat shock, HRG-7::mCherry was clearly visible in the pseudocoelom and coelomocytes but not within the intestine (Fig. 3a,b and Supplementary Fig. 3a) affirming that HRG-7 is secreted from the intestine shortly after protein translation.

To gain a better understanding of factors that regulate HRG-7 production and export, we RNAi-depleted 45 genes that encode known regulators of endocytosis and secretion in the $P_{vha\text{-}6}$*::HRG-7::mCherry* reporter strain[29]. We found that depletion of 11 trafficking factors caused HRG-7::mCherry to mis-localize (Supplementary Table 1). For example, depletion of genes encoding the SNARE (*snap-29*) or vacuolar ATPase (*vha-1*) components resulted in accumulation of HRG-7::mCherry either in the intestine (Fig. 3c) or as an immature form in which the pro-region was not cleaved (Fig. 3d). Consistent with aberrant HRG-7 secretion and processing, RNAi of *snap-29* also

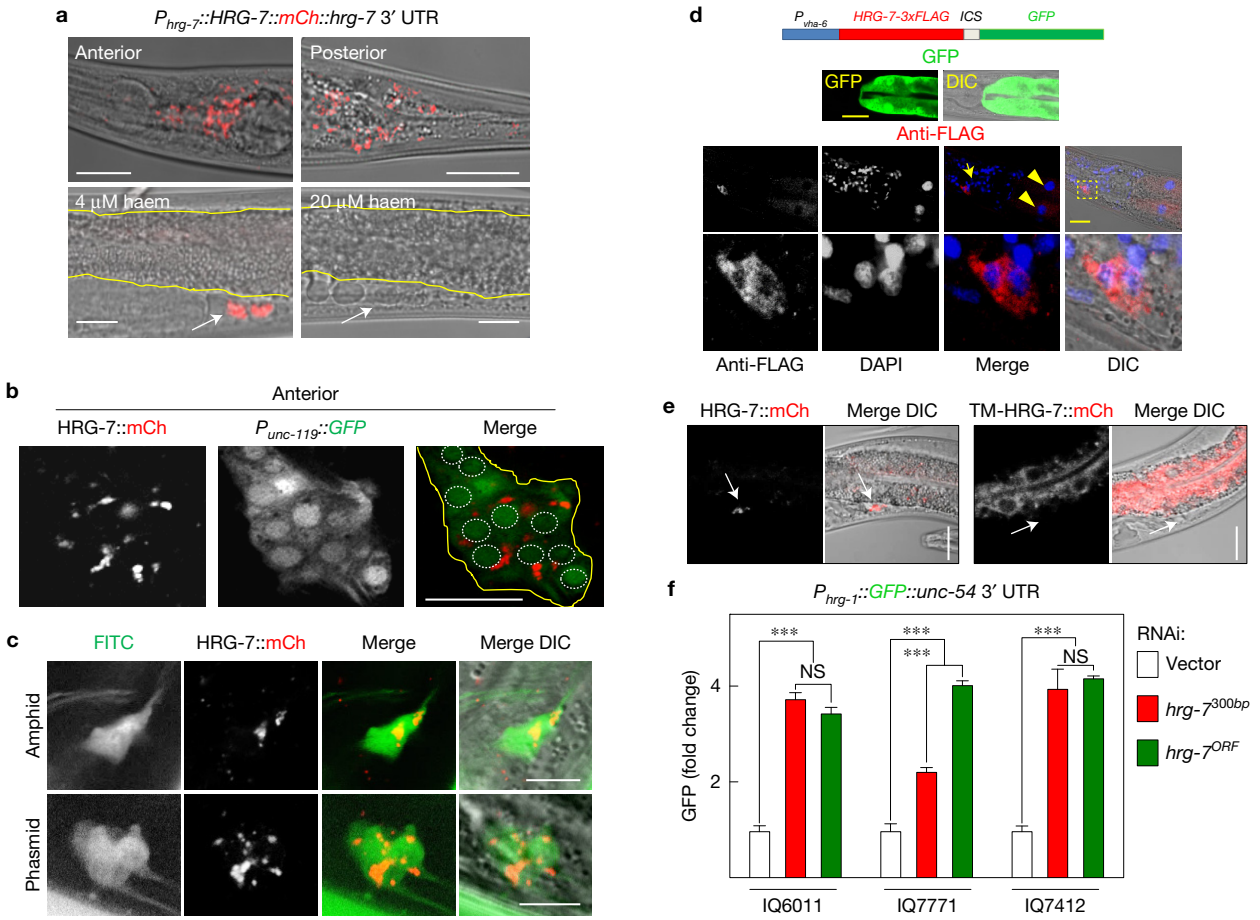

Figure 2 HRG-7 is secreted and functions in a cell-non-autonomous manner. (**a**) mCherry expression in IQ7777 ($P_{hrg\text{-}7}$*::HRG-7::mCherry*). Intestine is indicated by yellow lines; coelomocytes are indicated by a white arrow. Scale bars, 20 μm. Images are representative of three independent experiments. (**b**) Co-expression of the pan-neuronal GFP marker $P_{unc\text{-}119}$*::GFP* and $P_{vha\text{-}6}$*::HRG-7::mCherry*. The image is representative of the anterior of adults. The yellow outline indicates the nerve ring. White dotted circles indicate nerve ring nuclei. Scale bar, 10 μM. The images are representative of three independent experiments. (**c**) IQ7670 ($P_{vha\text{-}6}$*::HRG-7::mCherry*) were pulsed with 10 μg ml^{-1} FITC for 3 h, and then analysed by confocal microscopy. DIC, differential interference contrast. Scale bars, 5 μM. The images are representative of three independent experiments. (**d**) Fluorescence and immunofluorescence images of worms expressing $P_{vha\text{-}6}$*::HRG-7-3xFLAG::ICS::mCherry*. GFP expression was analysed in live worms. HRG-7-3xFLAG expression was analysed in fixed worms incubated with M2 anti-FLAG antibody followed by incubation with tetramethyl rhodamine 5 (and 6)-isothiocyanate (TRITC)-conjugated goat-anti-mouse antibody and DAPI. The arrow indicates neuron nuclei. The arrowheads indicate intestine nuclei. The bottom panels are zoomed-in images of the boxed region indicated in the middle panels. The images are representative of two independent experiments. Scale bars, 20 μm. (**e**) mCherry fluorescence in worms expressing $P_{vha\text{-}6}$*::HRG-7^{PR}::mCherry* or $P_{vha\text{-}6}$*::TM-HRG-7^{PR}::mCherry*. The arrows indicate middle coelomocytes near the vulva. Scale bars, 20 μm. The images are representative of three independent experiments. (**f**) GFP fluorescence quantified from IQ6011 ($P_{hrg\text{-}1}$*::GFP*), IQ7771 ($P_{vha\text{-}6}$*::HRG-7^{PR}::mCherry; $P_{hrg\text{-}1}$::GFP*) and IQ7412 ($P_{vha\text{-}6}$*::TM-HRG-7^{PR}::mCherry; $P_{hrg\text{-}1}$::GFP*) fed dsRNA against control vector, *hrg-7*^{300bp} and *hrg-7*^{ORF} at 10 μM haem. GFP was quantified using COPAS BioSort. GFP is presented as fold change compared with vector. The graph represents the mean and s.e.m. of three biologically independent experiments. $n = 120$ worms per treatment per experiment. $^{***}P < 0.001$ (one-way ANOVA). See Supplementary Table 3 for statistics source data.

resulted in increased GFP expression in the $P_{hrg\text{-}1}$*::GFP* haem sensor strain (Supplementary Fig. 5e). These results demonstrate that HRG-7 maturation and secretion require endosomal fusion and acidification. Because genetic disruption of the vacuolar ATPase complex can affect both secretory and acidification processes[30], we analysed the dynamics of HRG-7 maturation *in vitro*. Lysates from transgenic worms expressing $P_{vha\text{-}6}$*::HRG-7-3xFLAG* were exposed to either neutral or acidic pH at 25 °C for 20 min. While HRG-7-3xFLAG remained in the pro-form at pH 7.2, at pH 4 the majority of pro-HRG-7-3xFLAG was processed by cleavage within 20 min (Fig. 3e), supporting a role for an acidic environment for HRG-7 maturation.

To examine whether the intestinal source of HRG-7 could be substituted by expressing *hrg-7* either directly in the recipient tissue (neuron) or from another tissue (body wall muscle), we expressed *hrg-7*^{PR}*::ICS::mCherry* from the *unc-119* or *myo-3* promoters, respectively. The SL2 trans-spliced mCherry expression revealed that the transgene was indeed expressed in the appropriate tissue, but mature HRG-7 protein could be detected only when expressed from the intestine (Supplementary Fig. 3b,c). Consequently, only intestinal *hrg-7* was capable of restoring *GFP* expression in the $P_{hrg\text{-}1}$*::GFP* haem sensor worms (Supplementary Fig. 3d). Together, these results imply that the intestine is the sole tissue source of functional HRG-7.

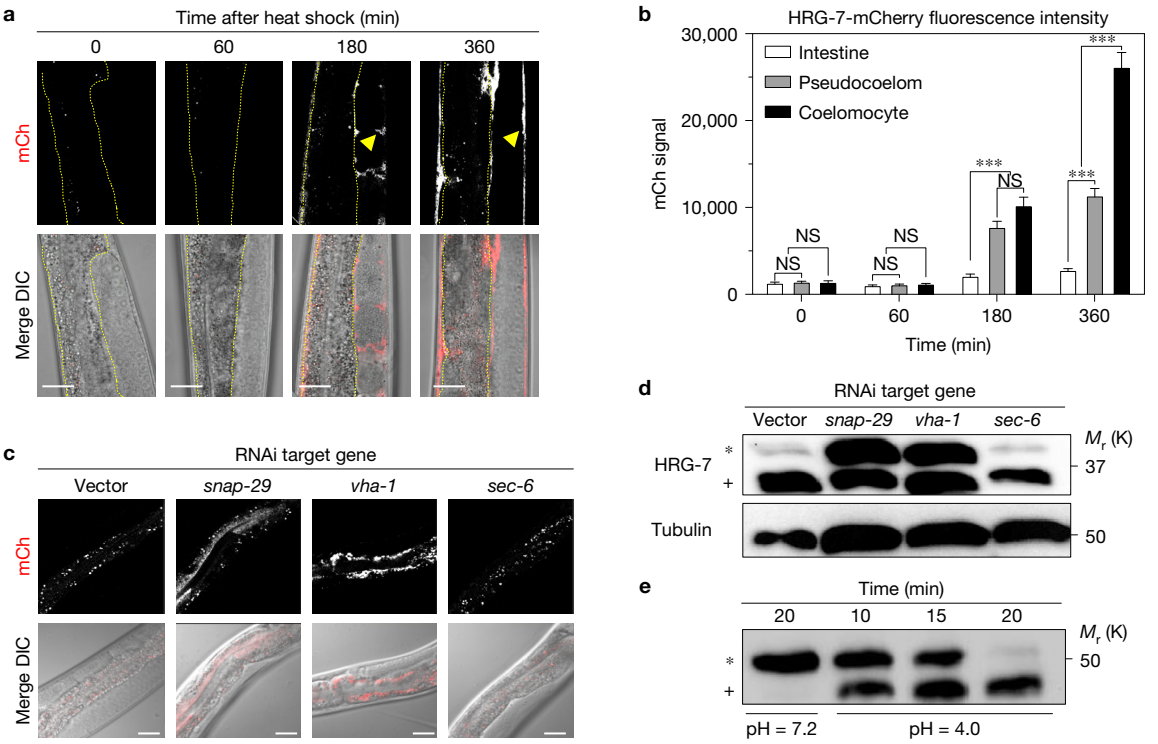

Figure 3 HRG-7 secretion and maturation is regulated by specific trafficking factors. (**a**) mCherry expression in strain IQ7170 ($P_{hsp-16.2}$*::HRG-7::mCherry*) placed at 37 °C for 30 min, then 20 °C for 60, 180 and 360 min. The dotted yellow lines outline the intestine. The arrowheads indicate HRG-7::mCherry in the pseudocoelom. Scale bars, 20 μm. Images are representative of three independent experiments. (**b**) Quantification of mCherry in coelomocytes, pseudocoelom and intestine of IQ7170 following heat shock. For quantification, 10 images, consisting of 10–15 *z*-stacks per image, were used for each time point. The graph represents the mean and s.e.m. $^{***}P < 0.001$ (two-way ANOVA). NS, not significant. mCherry signal is in arbitrary units. The graph and statistics are from a single experiment. The experiment was repeated one time with similar results. (**c**) mCherry expression in strain IQ7670 fed dsRNA against control vector, *snap-29*, *vha-1* and *sec-6*. The small puncta visible in all panels are autofluorescent gut granules in the intestine. Scale bars, 20 μm. Images are representative of three independent experiments. (**d**) Immunoblot analysis of strain N2 fed dsRNA against control vector, *snap-29*, *vha-1* and *sec-6*. Membranes were probed with polyclonal anti-HRG-7 antibody and then incubated with HRP-conjugated anti-rabbit secondary antibody. * indicates pro-HRG-7. + indicates mature HRG-7. Unprocessed original scans of blots are shown in Supplementary Fig. 6. Data are representative of three independent experiments. (**e**) Immunoblot analysis of lysate prepared from strain IQ7370 (P_{vha-6}*::HRG-7::3xFLAG*) at pH 7.2 and pH 4. Membranes were probed with monoclonal anti-FLAG antibody and then incubated with HRP-conjugated anti-mouse secondary antibody. * indicates pro-HRG-7-3xFLAG. + indicates mature HRG-7-3xFLAG. Unprocessed original scans of blots are shown in Supplementary Fig. 6. Data are representative of three independent experiments.

The haem-signalling function of HRG-7 does not require conserved active-site aspartates

The *hrg-7(tm6801)* mutant contains an in-frame deletion of 40 amino acids encompassing a conserved tyrosine flap shown to be critical for the function of aspartic proteases (Fig. 4a and Supplementary Fig. 4a,b). The *hrg-7(tm6801)* mutants have undetectable levels of functionally mature HRG-7 protein as identified by immunoblotting (Supplementary Fig. 4c). Longer exposure of the immunoblots revealed mutant HRG-7 migrating around the same molecular weight as the WT protein. This would be expected if the mutant HRG-7 retained the 30-amino-acid pro-peptide, offsetting much of the size reduction expected for a 40-amino-acid deletion. We speculate that the higher molecular weight band in the *hrg-7(tm6801)* mutant could be misfolded aggregates of mutant HRG-7. *hrg-7(tm6801)* worms showed a severe haem-dependent growth defect and a striking haem deficiency signal in the P_{hrg-1}*::GFP* haem sensor worms, phenotypes that were fully suppressed by co-expression of a transgene encoding the WT HRG-7 protein (Fig. 4b and Supplementary Fig. 4d). Importantly, quantitative real-time PCR (qRT-PCR) confirmed that endogenous *hrg-1* mRNA was also significantly upregulated in the *hrg-7(tm6801)* mutants (Fig. 4c), reproducing the GFP upregulation observed in the P_{hrg-1}*::GFP* haem sensor worms (Fig. 1e and Supplementary Fig. 4d).

Typical aspartic acid proteases utilize a catalytic dyad of two aspartic acids for proteolysis, a feature shared by other A1 aspartic protease family members that include cathepsin D, cathepsin E, pepsin and renin. *In silico* homology modelling predicts HRG-7 to be a bi-lobed structure with each lobe contributing an active site aspartic acid residue and a conserved disulfide bond (Supplementary Fig. 4b). To determine whether the signalling function of HRG-7 was dependent on these aspartic acids, we mutated Asp90 and Asp318 to alanines. Surprisingly, a D90A/D318A double mutant fully restored *GFP* expression to WT levels in the P_{hrg-1}*::GFP* haem sensor worms crossed into *hrg-7(tm6801)* mutants (Fig. 4d). Furthermore, the D90A/D318A mutant was comparable to WT in suppressing the growth defects of *hrg-7(tm6801)* mutants (Fig. 4e). The phenotypic rescue by the *D90A/D318A* allele was not due to overexpression of the transgene as the steady-state level of the mutant protein was even lower than endogenous HRG-7 (Supplementary Fig. 4e). Together,

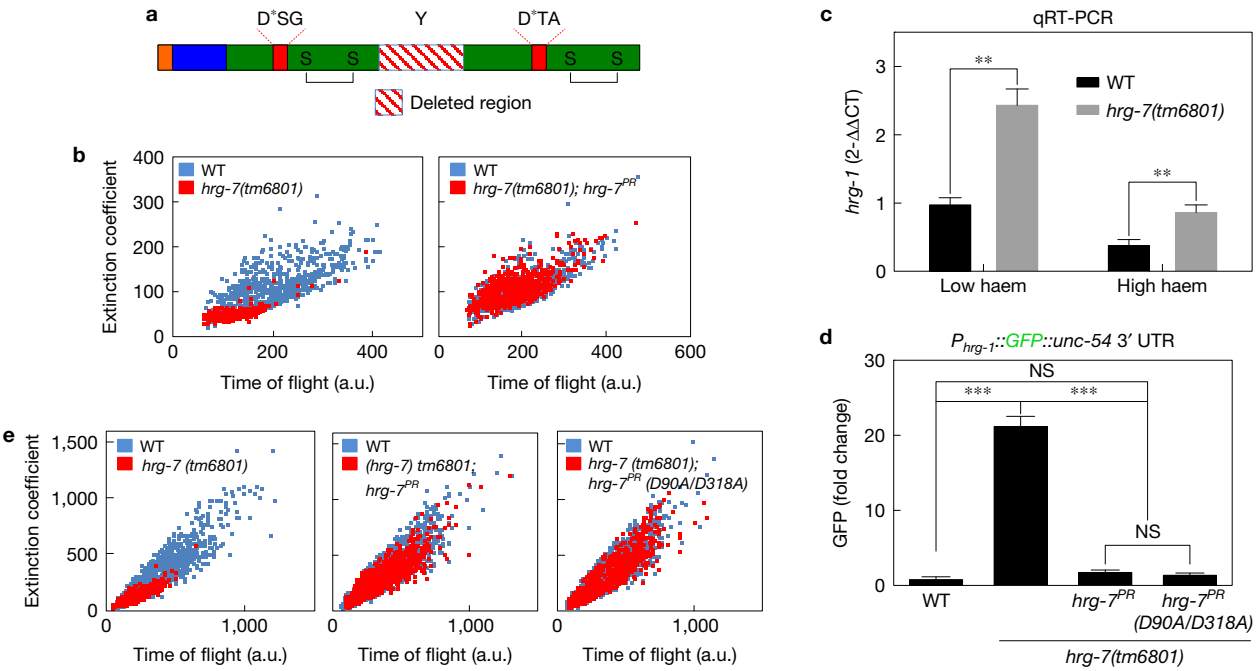

Figure 4 Conserved aspartic acid residues are dispensable for HRG-7 function in haem homeostasis. (**a**) Cartoon of HRG-7 depicting the truncation resulting from the *tm6801* allele, which encompasses the conserved tyrosine of the flap region. (**b**) Size quantification (400–800 worms per strain) of WT worms, *hrg-7(tm6801)* mutant worms or *hrg-7(tm6801)* mutants expressing transgenic $P_{vha\text{-}6}$*::hrg-7*^{PR} grown on RP523 bacteria supplemented with 1 μM haem for two generations. F1 worms were harvested as WT were becoming L4 larvae. The graph is representative of a single experiment. Two experiments were repeated independently with similar results. (**c**) qRT-PCR of *hrg-1* in *hrg-7(tm6801)* mutant worms or WT broodmates fed OP50 (low haem) or OP50 with 50 μM haem (high haem). The graph represents the mean and s.e.m. of three biologically independent experiments. *hrg-1* expression was normalized to *gpd-2*. Data are presented as fold change compared with *hrg-1* expression in WT broodmates grown with low haem. $^{**}P < 0.01$ (unpaired two-tailed *t*-test). See Supplementary Table 3 for statistics source data. (**d**) GFP fluorescence quantified from IQ6011 expressing WT *hrg-7*, *hrg-7(tm6801)*, *hrg-7(tm6801)* and transgenic $P_{vha\text{-}6}$*::hrg-7*^{PR}, or *hrg-7(tm6801)* and transgenic $P_{vha\text{-}6}$*::hrg-7*^{PR}*(D90A/D318A)* and grown on OP50. GFP was quantified using COPAS BioSort. GFP is presented as fold change compared with WT worms. The graph represents the mean and s.e.m. of three biologically independent experiments. $n = 120$ worms per treatment per experiment. $^{***}P < 0.001$ (one-way ANOVA). NS, not significant. See Supplementary Table 3 for statistics source data. (**e**) Size quantification of strains (500–1,000 worms per strain) from **d** grown on RP523 bacteria supplemented with 4 μM haem for two generations. Graph is representative of a single experiment. Two experiments were repeated independently with similar results.

these results demonstrate that HRG-7 is essential for haem-dependent growth and that the signalling function of HRG-7 is not dependent on conserved aspartates in the putative active site.

DBL-1 regulates *hrg-1* and *hrg-7* through neuron-to-intestine signalling

Our results show that intestinal HRG-7 is secreted and localizes distally to sensory neurons and that the loss of HRG-7, or obstructing its secretion, causes aberrant intestinal haem homeostasis. In *C. elegans*, the intestines are physically separated from most extra-intestinal tissues by the pseudocoelom, a fluid-filled body cavity that bathes the internal organs[31,32]. This raised the possibility that an extra-intestinal regulatory signal might reciprocally regulate intestinal haem homeostasis through a secreted, diffusible factor(s). To identify this regulatory factor, we screened 117 genes that represented 80% of the predicted secreted morphogens and neuropeptides in *C. elegans* using RNAi depletion in the RNAi hypersensitive haem sensor strain $P_{hrg\text{-}1}$*::GFP; lin-15b(n744)* (IQ6015). The *lin-15b*(*n744*) mutation allows for more efficient knockdown in tissues that are normally resistant to RNAi, such as some neurons and the pharynx[33]. Quantification of intestinal GFP fluorescence for each of the 117 gene knockdowns ($n = 120$ worms) using the COPAS Biosorter identified *dbl-1*, encoding a bone morphogenic protein-5 (BMP5) homologue, as the top hit (Fig. 5a and Supplementary Table 2). Consistent with our RNAi screen results and published microarray results from *dbl-1* mutant worms, *hrg-1* mRNA was significantly upregulated in *dbl-1(nk3)* mutant worms compared with WT broodmate controls (Fig. 5b)[34].

DBL-1 is a secreted signalling factor for which circulating levels of this morphogen are a better indicator of its function than tissue-specific expression levels[35]. Transcriptional reporter fusions expressing an integrated $P_{dbl\text{-}1}$*::GFP* transgene showed that *dbl-1* expression is restricted to neurons (Supplementary Fig. 5a)[36]. However, a *dbl-1::GFP* translational fusion has also been reported to be expressed in neurons as well as body wall muscles and the pharyngeal region[37], although we and others observe only neuronal expression (Supplementary Fig. 5a). Indeed, analyses of several integrated lines expressing a recently synthesized GFP-tagged DBL-1 showed only neuronal expression[38].

We analysed haem sensing in *dbl-1(nk3)* mutants using the $P_{hrg\text{-}1}$*::GFP* reporter gene. Loss of *dbl-1* resulted in an upregulation of intestinal $P_{hrg\text{-}1}$*::GFP* over a broad range of haem concentrations when compared with WT broodmates (Fig. 5c and Supplementary Fig. 5b). By contrast, overexpression of extrachromosomal copies of

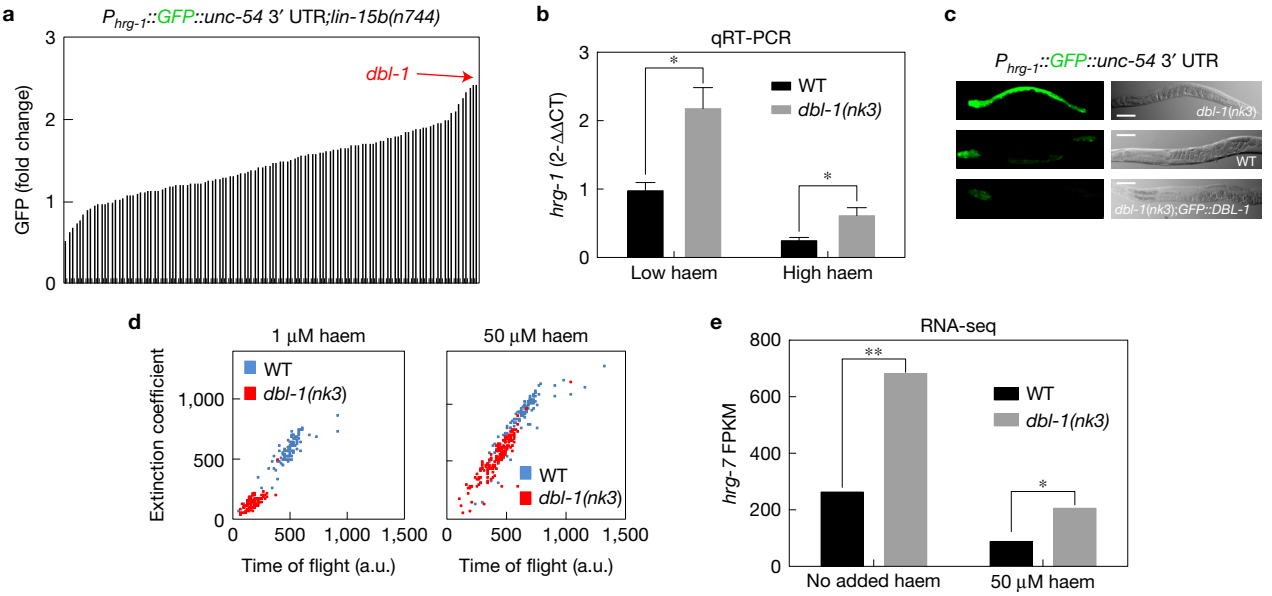

Figure 5 DBL-1 regulates *hrg-1* and *hrg-7* through neuron-to-intestine signalling. (**a**) GFP quantification (mean of 120 worms) in strain IQ6015 [P_{hrg-1}::*GFP; lin-15b(n744)*] fed dsRNA against 117 genes encoding secreted signalling factors. The *y* axis is GFP fold change compared with worms fed control vector. GFP was quantified using COPAS BioSort. (**b**) qRT-PCR of *hrg-1* in *dbl-1(nk3)* mutant worms or WT broodmates fed OP50 (low haem) or OP50 with 50 μM haem (high haem). The graph represents the mean and s.e.m. from five biologically independent experiments. *hrg-1* expression was normalized to *gpd-2*. Data are presented as fold change compared with *hrg-1* expression in WT broodmates grown with low haem. $^{*}P < 0.05$ (unpaired two-tailed *t*-test). See Supplementary Table 3 for statistics source data. (**c**) Fluorescence images of IQ6011, IQ6311 and IQ6312 grown on OP50. Scale bars, 20 μm. The images are representative of three independent experiments. (**d**) Size analyses (100–150 worms per treatment) quantified from IQ6011 and IQ6311 fed RP523 *E. coli* grown in 1 μM or 50 μM haem for 96 or 72 h, respectively. Size was analysed using COPAS BioSort. The graph is representative of a single experiment. Two experiments were repeated independently with similar results. (**e**) FPKM (fragments per kilobase of transcript per million mapped reads) values for *hrg-7* from RNA-seq of *dbl-1(nk3)* mutants compared with WT broodmates. The graph represents the mean of FPKM values obtained from two biologically independent experiments. $^{**}P < 0.01$, $^{*}P < 0.05$ (false discovery rate). See Supplementary Table 3 for statistics source data.

a transgene encoding GFP::DBL-1 suppressed P_{hrg-1}::*GFP* expression in the *dbl-1(nk3)* mutants. Notably, these worms showed an enhanced suppression of P_{hrg-1}::*GFP* expression in low haem conditions compared with WT broodmates, validating a published report that DBL-1 function is dose-dependent[37]. Furthermore, the *gfp::dbl-1* transgene expression was restricted to neurons and neuron support cells (Supplementary Fig. 5c), indicating that nervous system production of DBL-1 in the *dbl-1(nk3)* mutants is sufficient to restore *hrg-1*-mediated intestinal haem homeostasis (Supplementary Fig. 5b and Fig. 5c).

To evaluate haem-dependent growth phenotypes in *dbl-1(nk3)* mutants, worms were fed RP523, an *Escherichia coli* mutant unable to synthesize haem[23]. Worms lacking *dbl-1* activity were significantly and persistently growth retarded when grown on RP523 supplemented with 1 μM haem, a phenotype that was fully suppressed with 50 μM haem supplementation (Fig. 5d). RNA-seq analysis of total RNA extracted from *dbl-1(nk3)* mutants and the corresponding WT broodmate controls fed *E. coli* supplemented with or without haem showed significantly elevated levels of *hrg-7* mRNA in *dbl-1(nk3)* mutants (Fig. 5e); *hrg-1* mRNA was also elevated by this analysis in *dbl-1(nk3)* mutants, confirming the RT-qPCR results reported above.

Intestinal expression of *hrg-1* and *hrg-7* is regulated via the transcription factor SMA-9

To gain insight into how DBL-1 regulates intestinal *hrg-1* expression, we compared regulators that significantly altered P_{hrg-1}::*GFP* expression by ≥ 2-fold with known genetic interactors of *dbl-1*. Only one gene was found to be common in both data sets: that gene encodes the transcription factor SMA-9. Previously, *sma-9* has been shown to genetically interact with *dbl-1* to regulate body size[39], but unlike neuronal *dbl-1*, *sma-9* is expressed in most somatic tissue including the intestine (Supplementary Fig. 5d)[39]. RNAi depletion of *sma-9* phenocopied *dbl-1* RNAi in the upregulation of GFP in the P_{hrg-1}::*GFP* haem sensor worms (Fig. 6a,b), and in the P_{hrg-7}::*GFP* transcriptional reporter (Fig. 6c). Importantly, GFP upregulation by *sma-9* depletion was abrogated in *dbl-1(nk3)* mutants (Fig. 6a), and co-RNAi of *dbl-1* and *sma-9* did not show an additive effect on GFP levels (Fig. 6b). Together, these results imply a role for DBL-1 in the repression of *hrg-1* expression via *sma-9*.

DISCUSSION

In *C. elegans*, a natural haem auxotroph, organs must have a mechanism to communicate and coordinate their haem status with intestinal haem uptake and transport. In the current study, we have demonstrated that a haem-dependent, inter-organ communication system exists in *C. elegans* and that this system is facilitated by signalling between the intestine and neurons (Fig. 6d). The question arises as to how HRG-7 gets targeted to neurons. RNAi depletion of the *C. elegans* fibroblast growth factor (FGF) homologue, *let-756*, in the P_{hrg-1}::*GFP* haem sensor strain harbouring the *hrg-7 (tm6801)* mutation causes a significant increase in GFP (Supplementary Fig. 5e) consistent with

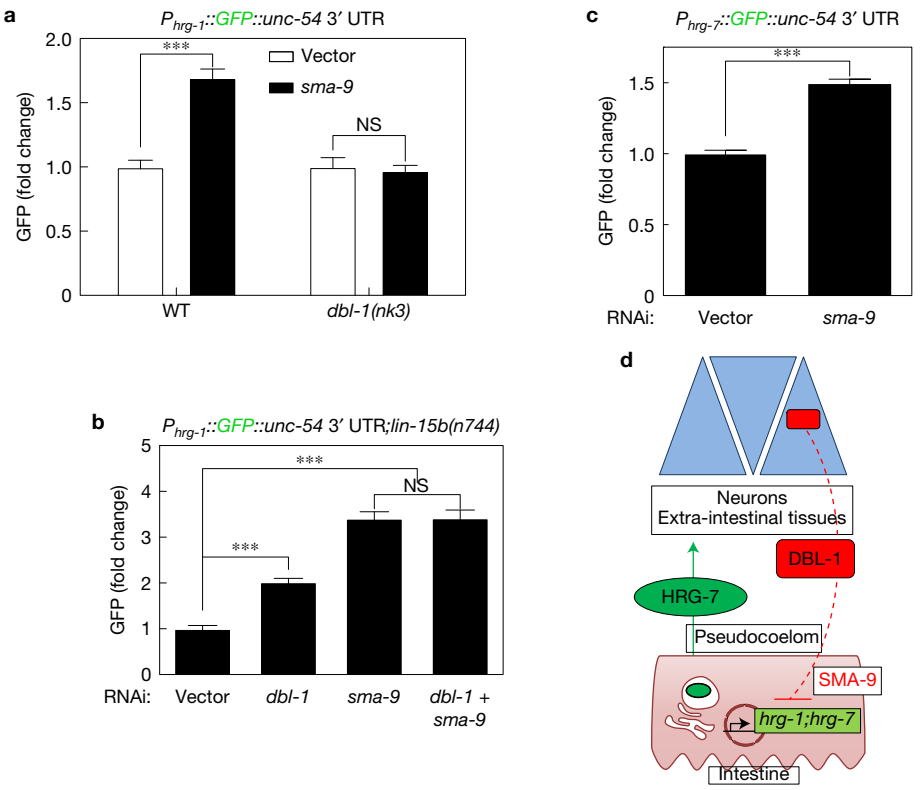

Figure 6 DBL-1 regulates *hrg-1* and *hrg-7* through SMA-9. (**a**) GFP fluorescence quantified from IQ6011 and IQ6311 fed vector control or dsRNA against *sma-9* at 10 μM haem. GFP was quantified using COPAS BioSort. GFP is presented as fold change compared with vector. The graph represents the mean and s.e.m. of three biologically independent experiments. $n = 120$ worms per treatment per experiment. $^{***}P < 0.001$ (unpaired two-tailed *t*-test). NS, not significant. See Supplementary Table 3 for statistics source data. (**b**) GFP fluorescence quantified from IQ6015 fed dsRNA against vector control, *dbl-1* or *sma-9* alone or in combination. GFP was quantified using COPAS BioSort. GFP is presented as fold change compared with vector. The graph represents the mean and s.e.m. of three biologically independent experiments. $n = 100$ worms per treatment per experiment. $^{***}P < 0.001$ (one-way ANOVA). NS, not significant. See Supplementary Table 3 for statistics source data. (**c**) GFP fluorescence quantified from IQ7701 worms fed dsRNA against vector control or *sma-9* at 25 μM haem. GFP was quantified using COPAS BioSort. GFP is presented as fold change compared with vector. The graph represents the mean and s.e.m. of three biologically independent experiments. $n = 120$ worms per treatment per experiment. $^{***}P < 0.001$ (unpaired two-tailed *t*-test). See Supplementary Table 3 for statistics source data. (**d**) Model of the inter-organ communication for organismal regulation of haem homeostasis. When haem conditions are sufficiently low, *hrg-1* and *hrg-7* expression is upregulated to ensure adequate haem distribution throughout the animal. HRG-7 leaves the intestine and is perceived by neurons either directly or indirectly. DBL-1 secreted from neurons represses *hrg-1* and *hrg-7* through a SMA-9-mediated pathway.

the possibility that LET-756 could directly interact with HRG-7 as demonstrated in a yeast two-hybrid screen[40]. Although intestines are capable of regulating haem transport in a cell-autonomous manner, evidence supports a role for neurons in systemic haem homeostasis. In *C. elegans*, sensory neurons are responsible for sensing nutrient availability and altering metabolism in peripheral tissues through an inter-tissue signalling pathway[26]. Furthermore, neuronal expression of haemoproteins such as soluble guanylate cyclases and globins dictates chemosensation and behavioural responses to food, oxygen and other animals[41,42]. Thus, it is conceivable that haem levels may alter behavioural responses to nutrient foraging and gas sensing in worms.

Our studies have also uncovered an unanticipated role for an aspartic protease homologue in haem homeostasis. Typically, aspartic proteases described in helminths are involved in digesting dietary proteins as a nutritional source[43,44], while we show that HRG-7 is secreted from the intestine to mediate inter-organ signalling. Several features of proteases make them attractive candidates for signalling. They are involved in interactions with their cognate substrates or inhibitors. Many are secreted. Some are inactive until removal of a pro-peptide allowing for a rapid cellular response to stimuli[45]. Our results also reveal that mutating the conserved aspartic acid residues in the putative active site has no effect on HRG-7-dependent signalling or growth, raising the possibility that HRG-7 proteolytic activity may be irrelevant. Indeed, functional, intact active site proteases can have signalling functions that are independent of their enzymatic activity[46]. For example, renin binds a receptor that activates downstream signalling independent of its proteolytic processing of angiotensinogen[47]. Cathepsin D has been shown to act as a mitogen in tumour cells even after the active site is abolished[48]. Since homologues for HRG-7, homologous to cathepsin E (ref. 49), DBL-1, homologous to BMP5, SMA-9, homologous to SHN and HRG-1, homologous to SLC48A1 are also present in mammals, it is conceivable that an analogous cell-non-autonomous signalling pathway may exist in humans to regulate iron and haem metabolism. □

METHODS

Methods, including statements of data availability and any associated accession codes and references, are available in the online version of this paper.

Note: Supplementary Information is available in the online version of the paper

ACKNOWLEDGEMENTS

We thank A. Chisholm, K. Liu, T. Gumienny, A. Jose and D. Hall for critical discussions and advice; T. Fukushige for preparing the RNA-seq libraries and extensive discussions; National Bioresource Project and S. Mitani (Tokyo Women's Medical University, Japan) for the *hrg-7* strain; H. Fares (University of Arizona, USA) for strain NP97 ($P_{unc\text{-}122}$::*GFP*). This work was supported by funding from the National Institutes of Health DK074797 and a supplement to DK074797 (I.H.); support was also provided by the Intramural Program of the National Institute of Diabetes and Digestive and Kidney Diseases (M.K.). The genome-wide RNAi screen was funded by the Roche Foundation for Anemia Research (I.H.).

AUTHOR CONTRIBUTIONS

Experimental design and execution were as follows: *C. elegans* experiments J.S., K.P., T.S., S.B., X.Y., J.Z., K.M., M.K. and I.H.; homology modelling and RNA-seq analyses S.Y.; J.S. and I.H. wrote the manuscript. All authors discussed the results and commented on the manuscript.

COMPETING FINANCIAL INTERESTS

I.H. is the President and Founder of Rakta Therapeutics Inc. (College Park, MD), a company involved in the development of haem transporter-related diagnostics.

Published online at http://dx.doi.org/10.1038/ncb3539

1. Hamza, I. Intracellular trafficking of porphyrins. *ACS Chem. Biol.* **1,** 627–629 (2006).
2. Severance, S. & Hamza, I. Trafficking of heme and porphyrins in metazoa. *Chem. Rev.* **109,** 4596–4616 (2009).
3. Korolnek, T. & Hamza, I. Macrophages and iron trafficking at the birth and death of red cells. *Blood* **125,** 2893–2897 (2015).
4. Keel, S. B. *et al.* A heme export protein is required for red blood cell differentiation and iron homeostasis. *Science* **319,** 825–828 (2008).
5. Cao, C. & O'Brien, K. O. Pregnancy and iron homeostasis: an update. *Nutr. Rev.* **71,** 35–51 (2013).
6. Yang, Z. *et al.* Kinetics and specificity of feline leukemia virus subgroup C receptor (FLVCR) export function and its dependence on hemopexin. *J. Biol. Chem.* **285,** 28874–28882 (2010).
7. Haldar, M. *et al.* Heme-mediated SPI-C induction promotes monocyte differentiation into iron-recycling macrophages. *Cell* **156,** 1223–1234 (2014).
8. Yuan, X. *et al.* Regulation of intracellular heme trafficking revealed by subcellular reporters. *Proc. Natl Acad. Sci. USA* **113,** E5144–E5152 (2016).
9. Sinclair, J. & Hamza, I. Lessons from bloodless worms: heme homeostasis in *C. elegans*. *Biometals* **28,** 481–489 (2015).
10. Rao, A. U., Carta, L. K., Lesuisse, E. & Hamza, I. Lack of heme synthesis in a free-living eukaryote. *Proc. Natl Acad. Sci. USA* **102,** 4270–4275 (2005).
11. Durieux, J., Wolff, S. & Dillin, A. The cell-non-autonomous nature of electron transport chain-mediated longevity. *Cell* **144,** 79–91 (2011).
12. Korolnek, T., Zhang, J., Beardsley, S., Scheffer, G. L. & Hamza, I. Control of metazoan heme homeostasis by a conserved multidrug resistance protein. *Cell Metab.* **19,** 1008–1019 (2014).
13. Rajagopal, A. *et al.* Haem homeostasis is regulated by the conserved and concerted functions of HRG-1 proteins. *Nature* **453,** 1127–1131 (2008).
14. Severance, S. *et al.* Genome-wide analysis reveals novel genes essential for heme homeostasis in *Caenorhabditis elegans*. *PLoS Genet.* **6,** e1001044 (2010).
15. Nemeth, E. *et al.* Hepcidin regulates cellular iron efflux by binding to ferroportin and inducing its internalization. *Science* **306,** 2090–2093 (2004).
16. Kim, B. E. *et al.* Cardiac copper deficiency activates a systemic signaling mechanism that communicates with the copper acquisition and storage organs. *Cell Metab.* **11,** 353–363 (2010).
17. Kautz, L. *et al.* Identification of erythroferrone as an erythroid regulator of iron metabolism. *Nat. Genet.* **46,** 678–684 (2014).
18. Sinclair, J. & Hamza, I. A novel heme response element mediates transcriptional regulation in *Caenorhabditis elegans*. *J. Biol. Chem.* **285,** 39536–39543 (2010).
19. McGhee, J. D. *et al.* The ELT-2 GATA-factor and the global regulation of transcription in the *C. elegans* intestine. *Dev. Biol.* **302,** 627–645 (2007).
20. Mahoney, T. R. *et al.* Intestinal signaling to GABAergic neurons regulates a rhythmic behavior in *Caenorhabditis elegans*. *Proc. Natl Acad. Sci. USA* **105,** 16350–16355 (2008).
21. Oka, T., Toyomura, T., Honjo, K., Wada, Y. & Futai, M. Four subunit a isoforms of *Caenorhabditis elegans* vacuolar H^+-ATPase. Cell-specific expression during development. *J. Biol. Chem.* **276,** 33079–33085 (2001).
22. Pujol, N., Bonnerot, C., Ewbank, J. J., Kohara, Y. & Thierry-Mieg, D. The *Caenorhabditis elegans unc-32* gene encodes alternative forms of a vacuolar ATPase a subunit. *J. Biol. Chem.* **276,** 11913–11921 (2001).
23. Chen, C., Samuel, T. K., Sinclair, J., Dailey, H. A. & Hamza, I. An intercellular heme-trafficking protein delivers maternal heme to the embryo during development in *C. elegans*. *Cell* **145,** 720–731 (2011).
24. Hedgecock, E. M., Culotti, J. G., Thomson, J. N. & Perkins, L. A. Axonal guidance mutants of *Caenorhabditis elegans* identified by filling sensory neurons with fluorescein dyes. *Dev. Biol.* **111,** 158–170 (1985).
25. Mak, H. Y., Nelson, L. S., Basson, M., Johnson, C. D. & Ruvkun, G. Polygenic control of *Caenorhabditis elegans* fat storage. *Nat. Genet.* **38,** 363–368 (2006).
26. Bishop, N. A. & Guarente, L. Two neurons mediate diet-restriction-induced longevity in *C. elegans*. *Nature* **447,** 545–549 (2007).
27. Evans, D. & Blumenthal, T. Trans splicing of polycistronic *Caenorhabditis elegans* pre-mRNAs: analysis of the SL2 RNA. *Mol. Cell. Biol.* **20,** 6659–6667 (2000).
28. Ding, L. & Candido, E. P. Association of several small heat-shock proteins with reproductive tissues in the nematode *Caenorhabditis elegans*. *Biochem. J.* **351,** 13–17 (2000).
29. Balklava, Z., Pant, S., Fares, H. & Grant, B. D. Genome-wide analysis identifies a general requirement for polarity proteins in endocytic traffic. *Nat. Cell Biol.* **9,** 1066–1073 (2007).
30. Poea-Guyon, S. *et al.* The V-ATPase membrane domain is a sensor of granular pH that controls the exocytotic machinery. *J. Cell Biol.* **203,** 283–298 (2013).
31. Wang, H. *et al.* Neuropeptide secreted from a pacemaker activates neurons to control a rhythmic behavior. *Curr. Biol.* **23,** 746–754 (2013).
32. Hung, W. L., Wang, Y., Chitturi, J. & Zhen, M. A *Caenorhabditis elegans* developmental decision requires insulin signaling-mediated neuron-intestine communication. *Development* **141,** 1767–1779 (2014).
33. Sieburth, D. *et al.* Systematic analysis of genes required for synapse structure and function. *Nature* **436,** 510–517 (2005).
34. Liang, J., Yu, L., Yin, J. & Savage-Dunn, C. Transcriptional repressor and activator activities of SMA-9 contribute differentially to BMP-related signaling outputs. *Dev. Biol.* **305,** 714–725 (2007).
35. Savage-Dunn, C., Yu, L., Gill, K., Awan, M. & Fernando, T. Non-stringent tissue-source requirements for BMP ligand expression in regulation of body size in *Caenorhabditis elegans*. *Genet. Res. (Camb)* **93,** 427–432 (2011).
36. Suzuki, Y. *et al.* A BMP homolog acts as a dose-dependent regulator of body size and male tail patterning in *Caenorhabditis elegans*. *Development* **126,** 241–250 (1999).
37. Morita, K., Chow, K. L. & Ueno, N. Regulation of body length and male tail ray pattern formation of *Caenorhabditis elegans* by a member of TGF-β family. *Development* **126,** 1337–1347 (1999).
38. Schultz, R. D., Bennett, E. E., Ellis, E. A. & Gumienny, T. L. Regulation of extracellular matrix organization by BMP signaling in *Caenorhabditis elegans*. *PLoS ONE* **9,** e101929 (2014).
39. Liang, J. *et al.* The *Caenorhabditis elegans* schnurri homolog sma-9 mediates stage- and cell type-specific responses to DBL-1 BMP-related signaling. *Development* **130,** 6453–6464 (2003).
40. Popovici, C. *et al.* Direct and heterologous approaches to identify the LET-756/FGF interactome. *BMC Genomics* **7,** 105 (2006).
41. Persson, A. *et al.* Natural variation in a neural globin tunes oxygen sensing in wild *Caenorhabditis elegans*. *Nature* **458,** 1030–1033 (2009).
42. Gray, J. M. *et al.* Oxygen sensation and social feeding mediated by a *C. elegans* guanylate cyclase homologue. *Nature* **430,** 317–322 (2004).
43. Williamson, A. L. *et al.* A multi-enzyme cascade of hemoglobin proteolysis in the intestine of blood-feeding hookworms. *J. Biol. Chem.* **279,** 35950–35957 (2004).
44. Brinkworth, R. I., Prociv, P., Loukas, A. & Brindley, P. J. Hemoglobin-degrading, aspartic proteases of blood-feeding parasites: substrate specificity revealed by homology models. *J. Biol. Chem.* **276,** 38844–38851 (2001).
45. Turk, B., Turk, D. & Turk, V. Protease signalling: the cutting edge. *EMBO J.* **31,** 1630–1643 (2012).
46. Rawlings, N. D., Waller, M., Barrett, A. J. & Bateman, A. MEROPS: the database of proteolytic enzymes, their substrates and inhibitors. *Nucleic Acids Res.* **42,** D503–D509 (2014).
47. Cousin, C., Bracquart, D., Contrepas, A. & Nguyen, G. Potential role of the (pro)renin receptor in cardiovascular and kidney diseases. *J. Nephrol.* **23,** 508–513 (2010).
48. Glondu, M. *et al.* A mutated cathepsin-D devoid of its catalytic activity stimulates the growth of cancer cells. *Oncogene* **20,** 6920–6929 (2001).
49. Ueno, E., Sakai, H., Kato, Y. & Yamamoto, K. Activation mechanism of erythrocyte cathepsin E. Evidence for the occurrence of the membrane-associated active enzyme. *J. Biochem.* **105,** 878–882 (1989).

DOI: 10.1038/ncb3539

METHODS

Animal model. Worms were maintained in liquid mCeHR-2 or on Nematode Growth Medium agar plates. Experiments were not randomized, and the investigators were not blinded to allocation during experiments and outcome assessment. Adult hermaphrodites were used for analyses unless noted otherwise.

Cell lines. No cell lines were used in this study.

RNAi interference by feeding. RNAi was performed as previously described[14]. For evaluation of GFP expression, GFP levels in gravid adults were observed visually using a Leica Microsystems MZ16FA stereoscope. The intensity and pattern of GFP in gravid worms feeding on bacteria producing dsRNA against each library clone was compared with the intensity and pattern of GFP in same-stage worms feeding on bacteria transformed with the empty vector. Three parameters were quantified with COPAS BioSort: time of flight (length), extinction (optical density) and GFP intensity. GFP intensity was normalized to time of flight.

GFP quantification using COPAS BioSort. Worms were rinsed off NGM plates or pelleted in axenic media and washed three times with M9 buffer. Forty to fifty worms suspended in 100 µl M9 buffer were placed in individual wells of a 96-well plate, which was then analysed with the COPAS BioSort. Photo-multiplier tube settings were 400 volts for IQ7701 and IQ6015, and 200 volts for all other strains in this study. GFP data obtained from the COPAS are presented as relative GFP on a scale from 1–100, or fold change compared with controls. The list of 177 genes determined to regulate $P_{hrg\text{-}1}$*::GFP* by COPAS analyses can be found in Supplementary Table 4.

Cloning. To generate the $P_{hrg\text{-}7}$*::GFP* transcriptional fusion, ~0.7 kb of the 5′ flanking region of *hrg-7* was ligated into the HindIII and BamHI restriction sites within the multiple cloning sequence of Fire vector pPD95.67. All other constructs were generated using Multisite Gateway recombination (Invitrogen). Promoters, coding regions, and 3′ untranslated regions were amplified with sequence-specific Gateway attb primers. PCR products were first recombined into donor plasmids, and then three donor plasmids were recombined into expression plasmids, according to the manufacturer's instructions (Invitrogen).

Generation of transgenic worms. Reporter constructs mixed in a 2:1 ratio with the *unc-119* rescue construct (18 µg total DNA) were introduced into *unc-119(ed-3)* worms by microparticle bombardment using the PDS-1000 particle delivery system (Bio-Rad). Transgenic lines were isolated after two weeks.

Immunoblotting. For detection of HRG-7 or HRG-7-3xFLAG, between 2,500 and 5,000 gravid or young adult worms were lysed in phosphate-buffered saline (PBS) with protease inhibitors (1 mM phenylmethylsulfonyl fluoride, 4 mM benzamidine, 2 µg ml^{-1} leupeptin, and 1 µg ml^{-1} pepstatin) and Lysing Matrix C beads (MP Biomedicals) in a FastPrep-24 Beadbeater (MP Biomedicals). Worm lysates were centrifuged 3 times at 10,000*g* for 10 min, and then total protein concentration in the supernatants was measured using the Pierce BCA assay kit (Thermo Scientific). Unboiled samples were mixed with Laemmli sample buffer and 50 µg protein per lane was separated on a 10% SDS–PAGE gel and transferred to a nitrocellulose membrane. The membrane was incubated overnight in 4 °C with anti-HRG-7 polyclonal antibody custom produced in rabbits by Thermo Scientific Pierce Protein Research or M2 anti-FLAG monoclonal antibody (Sigma, no. F3165) at a concentration of 1:1,000. Goat anti-rabbit HRP-conjugated secondary was used for anti-HRG-7, or rabbit anti-mouse HRP-conjugated secondary for anti-FLAG at a 1:10,000 dilution, and blots were developed in SuperWest Pico Chemiluminescent Substrate (Thermo Scientific). Bio-Rad Image Lab software was used to quantify blots.

DiI, FITC pulse. To stain amphid and phasmid neurons, worms were removed from plates with M9, washed twice with M9, and resuspended in 100 µl M9. A stock solution of 2 mg ml^{-1} 5-fluorescein isothiocyanate (FITC) in dimethylsulfoxide was diluted 1:200 into the mixture. The tubes were wrapped in aluminium foil to avoid light exposure and incubated for 3 h at room temperature. The worms were washed three times with M9 to remove excess dye, then immobilized in 10 mM levamisole on a 2% agarose pad and imaged by fluorescence microscopy using a Zeiss LSM710 laser scanning confocal microscope.

Haem response assay. Haemin chloride (Frontier Scientific) was dissolved in 0.3 M ammonium hydroxide to a stock concentration of 10 mM. For haem response assays, eggs were obtained from worm strains maintained in mCeHR-2 medium with 20 µM haem or on NGM plates seeded with OP50. The following day, synchronized L1 larvae were placed in mCeHR-2 medium or on NGM plates seeded with OP50 supplemented with varying haem concentrations. After 72 h, GFP or mCherry fluorescence was quantified with the COPAS BioSort and analysed by fluorescent microscopy.

***C. elegans* growth on RP523 bacteria.** The haem-deficient *E. coli* strain RP523 was grown overnight in LB supplemented with 4 µM haem[50]. The following day, cultures were placed in fresh LB with 1 µM or 50 µM haem and grown for 5.5 h to an $OD_{600\,nm}$ of 0.2. Cultures were seeded on NGM agar plates overnight. The following day, synchronized L1 larvae were placed on the RP523-seeded plates and incubated at 20 °C until analyses.

HRG-7 recoding. To generate *hrg-7* RNAi-resistant transgenes, the first 300 bp of endogenous sequence was recoded by base pair substitution at degenerate sites using the *C. elegans* codon adapter[51] and the Genscript rare codon usage tool (http://www.genscript.com/cgi-bin/tools/rare_codon_analysis)[51]. Any remaining contiguous stretches of six identical nucleotides between the recoded and endogenous sequences were changed manually, where applicable, to ensure RNAi resistance. The sequences were then sent to Genscript for synthesis.

Worm lysate acid titration. To evaluate HRG-7 processing, IQ7370 ($P_{vha\text{-}6}$*::HRG-7::3xFLAG*) worms were lysed in PBS + 1% *n*-dodecyl β-D-maltoside (DDM). The pH of each sample was lowered with acetate solution (1 part 0.2 M sodium acetate and 9 parts 0.2 M glacial acetic acid). The pH was brought to 8.0 with 0.1 M NaOH before running samples on a sodium dodecyl sulfate polyacrylamide gel electrophoresis (SDS–PAGE) gel.

Heat shock and coelomocyte mCherry quantification. Synchronized L1 worms expressing $P_{hsp\text{-}16.2}$::HRG-7::mCherry (IQ7170) were placed on NGM plates seeded with OP50. After 72 h, the plates were placed in a 37 °C incubator for 30 min. The plates were then transferred to a 20 °C incubator for 0, 60, 180 or 360 min. At the end of the time course, worms were washed off the plates with M9 and placed on ice. mCherry fluorescence was analysed using a Zeiss LSM 710 confocal microscope. For quantification of mCherry fluorescence in coelomocytes, coelomocyte boundaries were established on merged *z*-stack DIC images. The corresponding area of fluorescence images was quantified using the Region of Interest (ROI) Function in Zeiss Zen software. A ROI of equal volumetric area to the area of a coelomocyte was used to quantify mCherry in the pseudocoelom and intestine. Ten images, consisting of about 10–15 *z*-stacks per image, were used for each time point.

ZnMP uptake. To assess uptake of ZnMP, synchronized L1 worms were grown on NGM plates seeded with OP50 or RNAi bacteria until they reached L4 stage. Worms were washed off plates and rinsed three times in M9 buffer to remove bacteria. Worms were incubated in mCeHR-2 medium with 10 µM ZnMP overnight, rinsed to remove excess ZnMP, and imaged as described previously[10]. Briefly, worms were paralysed with 10 mM levamisole and imaged using a Leica DMIRE2 epifluorescence/DIC microscope. Images were obtained using a Retiga 1300 cooled mono 12-bit camera and quantified using SimplePCI software (Compix).

RNA-seq. Total RNA was extracted from 30,000 late L4 worms per condition using the Trizol method. cDNA libraries were constructed with the TruSeq kit (Illumina). Single-end 50 base reads were generated using a HiSeq 2500 (Illumina) and aligned to ce10 reference genome using Tophat2, version 2.1.0. Differentially expressed genes were found using Cufflinks 2, version 2.2.1 with the cutoff of 0.05 on false discovery rate.

Immunofluorescence. A mixed stage population were fixed and stained as previously described[52]. Incubation with primary M2 anti-FLAG antibody (Sigma, no. F3165) was followed by incubation with secondary tetramethyl rhodamine 5 (and 6)-isothiocyanate (TRITC)-conjugated goat anti-mouse antibody (Jackson ImmunoResearch).

qRT-PCR. RNA was isolated from 10,000 late L4 worms per condition using the Trizol method. cDNA was synthesized using SuperScript III First-Strand Synthesis System (Invitrogen). qRT-PCR was performed with SsoAdvanced Universal SYBR Green Supermix (Bio-Rad). Results were normalized with the CT value of *gpd-2*. Relative fold changes in *hrg-1* expression were determined using the 2-ΔΔCt calculations based on average CT values. Primers used were 5′qCehrg-1 AATGGCAGGATGGTCAGAAAC, 3′qCehrg-1 CGATGAATGAAA GGAACGATACG, 5′qgpd-2 TGCTCACGAGGGAGACTAC, 3′qgpd-2CGGTGG ACTCAACGACATAG.

Bioinformatics. Protein and DNA alignments were performed using ClustalW2 (http://www.ebi.ac.uk/Tools/msa/clustalw2). Signal peptides were predicted with the

SignalP 4.1 server (http://www.cbs.dtu.dk/services/SignalP). Interaction networks were analysed with geneMANIA (www.genemania.org). Homology models were generated with I-TASSER (http://zhanglab.ccmb.med.umich.edu/I-TASSER).

Statistics and reproducibility. Statistical significance was determined with GraphPad Prism, version 7.02 (GraphPad Software). Statistical significance for RNA-seq was determined by Cufflinks 2, version 2.2.1 with the cutoff of 0.05 on false discovery rate. Statistical tests are justified. No statistical method was used to predetermine sample size. All data are presented as the mean ± the standard error of the mean. Data meet the assumptions of the tests. Variance is similar among compared groups. For *C. elegans* quantification data, the number of times each experiment was repeated is stated in the figure legends. RNAi screens were performed one time, and candidate genes were validated at least three other times. For western blots, immunofluorescence, and transgenic expression data, all experiments were performed at least two times.

Code availability. Bioinformatic analysis using Clustalw is available at http://www.ebi.ac.uk/Tools/msa/clustalw2. Network analysis of *dbl-1* with GeneMania is available at http://genemania.org by using the search term '*dbl-1*'.

Data availability. RNA-Seq data have been deposited in the Gene Expression Omnibus (GEO) under accession code GSE76455. Source data for Figs 1a,e, 2f, 4c,d, 5b,e and 6a–c, and Supplementary Figs 2a,f, 3d and 4d have been provided as Supplementary Table 3. All other data supporting the findings of this study are available from the corresponding author on request.

50. Li, J. M., Umanoff, H., Proenca, R., Russell, C. S. & Cosloy, S. D. Cloning of the *Escherichia coli* K-12 hemB gene. *J. Bacteriol.* **170,** 1021–1025 (1988).
51. Redemann, S. *et al.* Codon adaptation-based control of protein expression in *C. elegans*. *Nat. Methods* **8,** 250–252 (2011).
52. Finney, M. & Ruvkun, G. The unc-86 gene product couples cell lineage and cell identity in *C. elegans*. *Cell* **63,** 895–905 (1990).

nature cell biology

DOI: 10.1038/ncb3539

In the format provided by the authors and unedited.

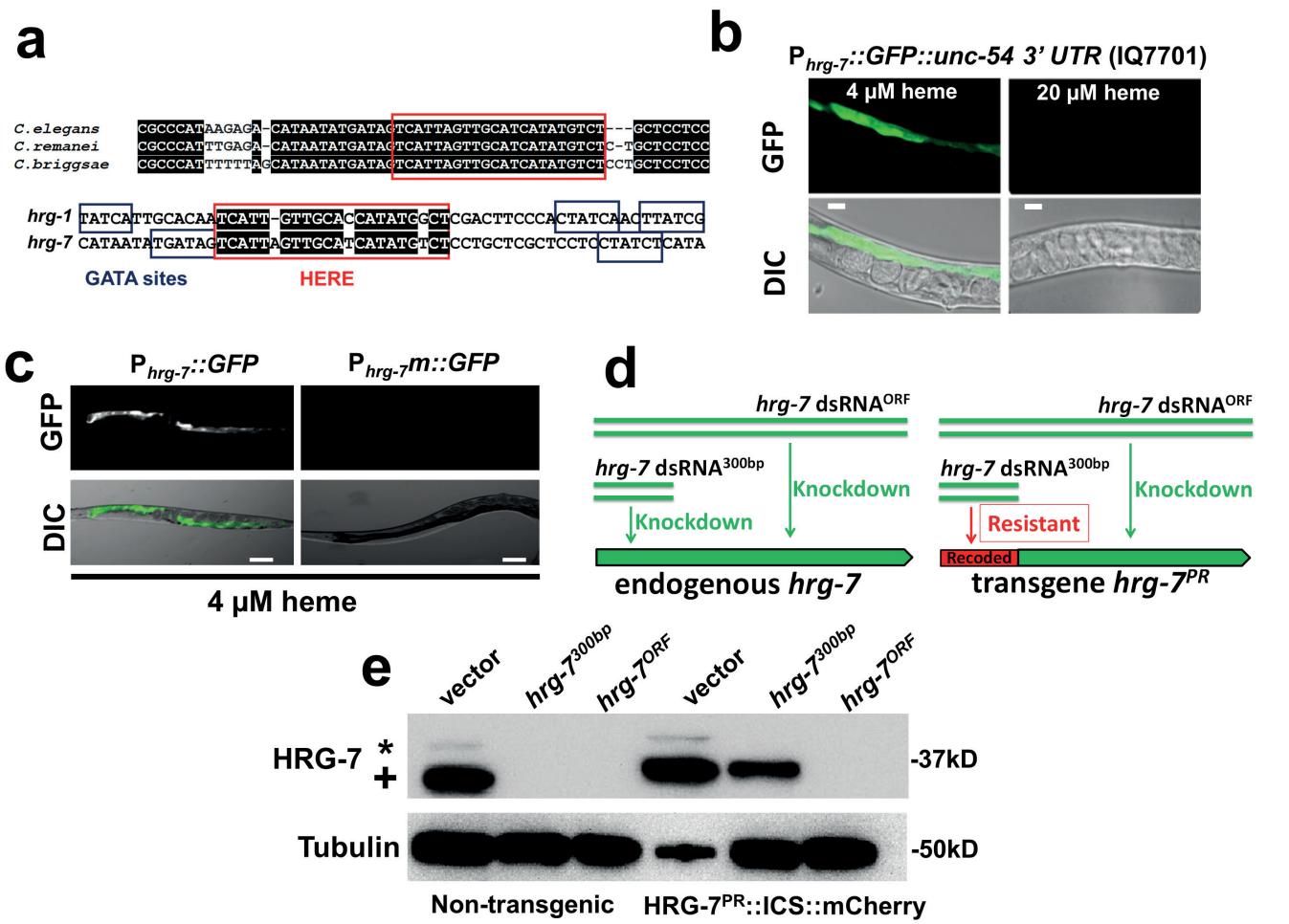

Supplementary Figure 1 Intestinal *hrg-7* is a regulator of heme homeostasis **a)** Top: ClustalW alignment of the *hrg-7* 5' flanking region with homologous sequences in *C. briggsae* and *C. remanei*. White text with black background indicates a conserved nucleotide in all three species. Red box indicates HERE. Bottom: Alignment of the *hrg-1* transcriptional regulatory region with the putative *hrg-7* transcriptional regulatory region. Red box indicates HERE. White text with black background indicates conserved nucleotides in the HERE. Blue boxes indicate GATA sites. **b)** GFP expression in strain IQ7701 ($P_{hrg\text{-}7}$*::GFP*) grown in 4 or 20 µM heme. Scale bar = 20 µm. Images are representative of three independent experiments. **c)** GFP expression in IQ7701 and IQ7702 ($P_{hrg\text{-}7}$*mut::GFP*) in 4 µM heme. GFP was only detectable in IQ7701. Images are representative of three independent experiments. **d)** Schematic showing that endogenous *hrg-7* is knocked down by both *hrg-7* dsRNA^{300bp} and *hrg-7* dsRNA^{ORF}, whereas the transgene *hrg-7*^{PR} is resistant to knockdown by *hrg-7* dsRNA^{300bp} but not to knockdown by *hrg-7* dsRNA^{ORF}. **e)** Immunoblot analysis of HRG-7 and HRG-7^{PR} from IQ6011 and IQ7711 fed dsRNA against control vector, *hrg-7*^{300bp}, and *hrg-7*^{ORF}. Membranes were probed with polyclonal anti-HRG-7 antibody and then incubated with HRP-conjugated anti-rabbit secondary antibody. * indicates pro-HRG-7. + indicates mature HRG-7. Unprocessed blots are shown in Figure S6. Data is representative of two independent experiments.

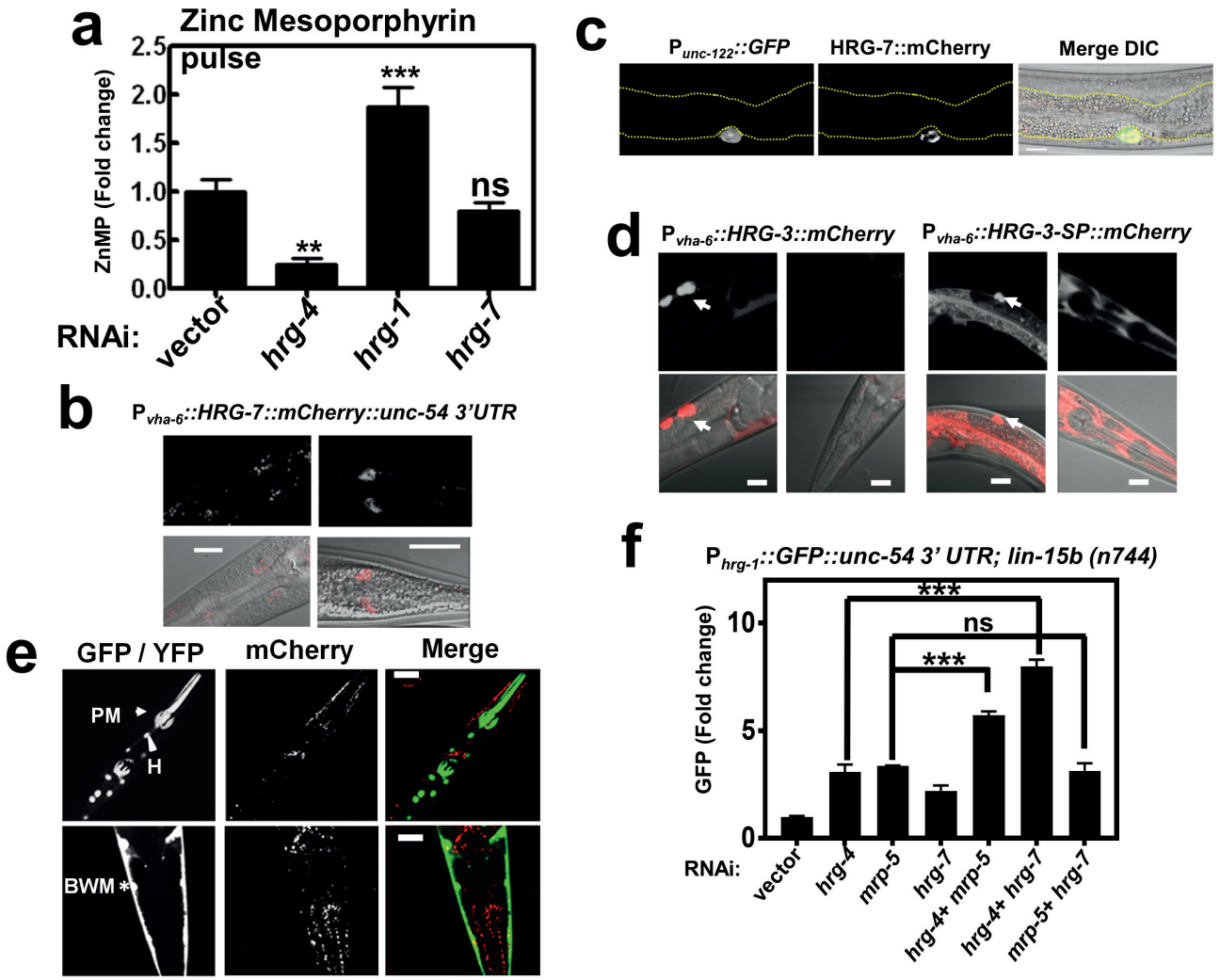

Supplementary Figure 2 Secreted HRG-7 exhibits a tissue specific localization pattern **a)** ZnMP staining in worms fed dsRNA against vector control, *hrg-4*, *hrg-1*, or *hrg-7*. Worms were exposed to RNAi from L1 to L4 larval stages, then pulsed with 10 mM ZnMP overnight. ZnMP staining was quantified using the region of interest function of Simple PCI. ZnMP intensity is presented as fold change compared to vector. Graph represents the mean and SEM of three biological independent experiments. N=10 worms per treatment per experiment. ***P<0.001, **P<0.01, *P<0.05, when compared to control worms (one-way ANOVA). See Supplementary Table 3 for statistics source data. **b)** mCherry expression in the anterior (left panel) and posterior (right panel) of strain IQ7670 (P_{vha-7}*::HRG-7::mCherry*). Scale bar = 20 µm. Images are representative of three independent experiments. **c)** Coexpression of the coelomocyte marker *Punc-*$_{122}$*::GFP* and P_{vha-6}*::HRG-7::mCherry.* Image depicts a middle coelomocyte. Scale bar = 20µm**.** Images are representative of three independent experiments. **d)** Left panels: mCherry expression in the gonad and coelomocytes of IQ8333 (P_{vha-6}*::HRG-3::mCherry*). No mCherry is observed in the anterior of the worm. Right panels: mCherry expression in the intestine, coelomocytes, and anterior of strain IQ8330 (P_{vha-6}*::HRG-3-SP::mCherry*). In the anterior of the worm, mCherry is non-specifically diffused throughout the pseudocoelomic fluid. Scale bar =20µm. Images are representative of three independent experiments. **e)** Representative images of tissue specific expression of GFP / YFP markers P_{ceh-22}*::GFP* (pharyngeal muscle), P_{dpy-7}*::YFP* (hypodermis), and P_{myo-2}*::GFP* (body wall muscle) crossed into strain IQ7670 (P_{vha-6}*::HRG-7::mCherry*). * indicates body wall muscle (BWM). Arrow indicates pharyngeal muscle (PM). Arrowhead indicates hypodermis (H). Scale bar =20µm. Images are representative of three independent experiments. **f)** GFP fluorescence quantified from IQ6015 [(P_{hrg-1}*::GFP*; *lin-15b*(*n744*)] fed dsRNA against control, *hrg-4*, *mrp-5*, or *hrg-7* alone or in combination. GFP was quantified using COPAS BioSort. GFP is presented as fold change compared to vector. Graph represents the mean and SEM of three biological independent experiments. N=120 worms per treatment per experiment. ***P<0.001, **P<0.01, *P<0.05 (one-way ANOVA). See Supplementary Table 3 for statistics source data.

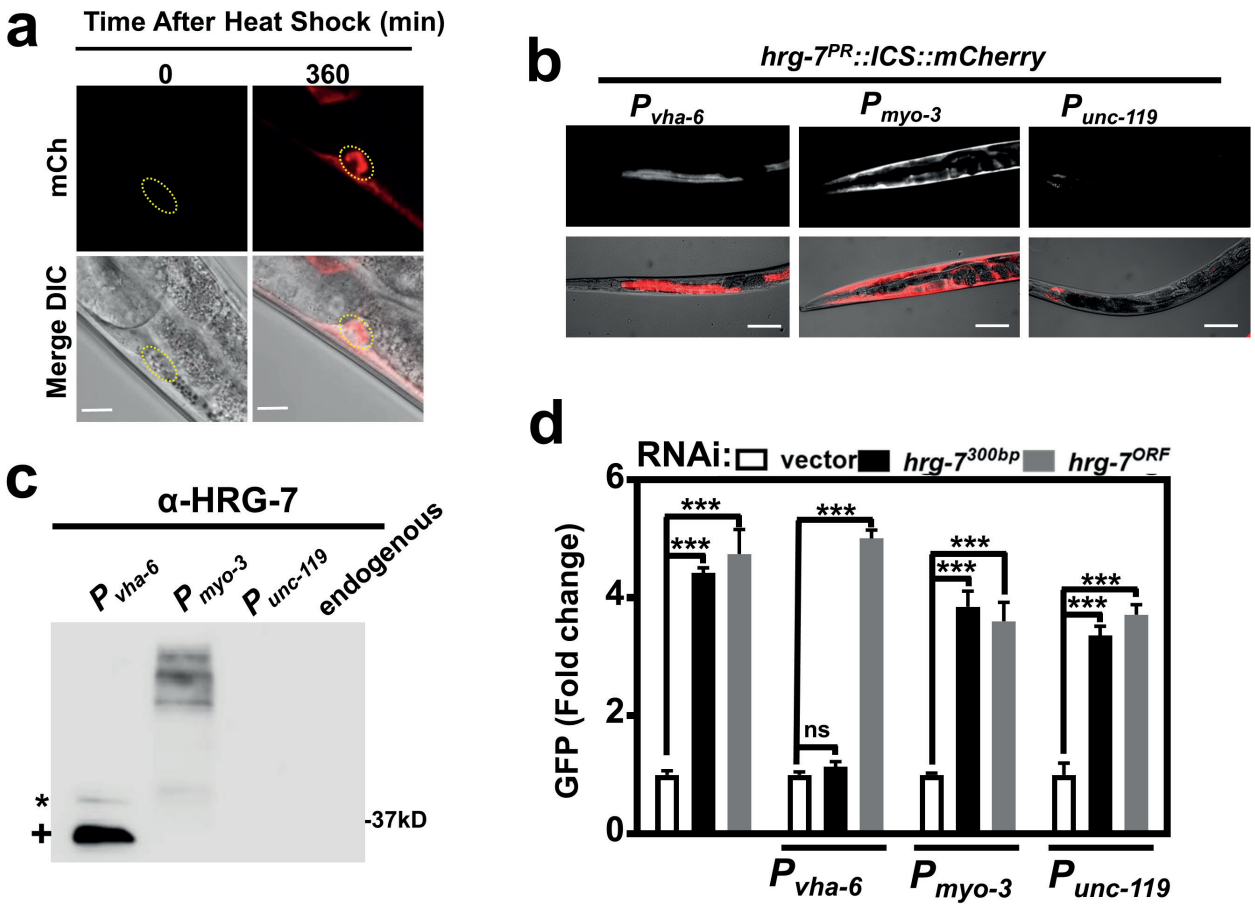

Supplementary Figure 3 Functional HRG-7 cannot be expressed by extraintestinal tissues **a)** Images of strain IQ7170 ($P_{hsp\text{-}16.2}$*::HRG-7-mCherry*) at timepoint= 0 and 360 minutes after heat shock. Coelomocytes are outlined by a yellow circle. Scale bar = 10 µm. **b)** Fluorescence images of worms expressing *hrg-7*$^{PR::}$*ICS::mCherry* from the *vha-6* (intestine), *myo-3* (muscle), or *unc-119* (neuron) promoter. **c)** Immunoblot analysis of HRG-7^{PR} expressed from the *vha-6*, *myo-3*, or *unc-119* promoter. Transgenic worms were fed dsRNA against *hrg-7*^{300bp}. Membranes were probed with polyclonal anti-HRG-7 antibody and then incubated with HRP-conjugated anti-rabbit secondary antibody. * indicates pro-HRG-7. + indicates mature HRG-7. Unprocessed blots are shown in Figure S6. Data is representative of two independent experiments. **d)** GFP fluorescence quantified from IQ6011 ($P_{hrg\text{-}1}$*::GFP*) or worms expressing $P_{hrg\text{-}1}$*::GFP* and HRG-7^{PR} from the *vha-6*, *myo-3*, or *unc-119* promoter fed dsRNA against control vector, *hrg-7*^{300bp}, and *hrg-7*^{ORF} at 10 µM heme. GFP was quantified using COPAS BioSort. GFP is presented as fold change compared to vector. Graph represents the mean and SEM of three biological independent experiments. N=120 worms per treatment per experiment. ***P<0.001, **P<0.01, *P<0.05 (one-way ANOVA)). See Supplementary Table 3 for statistics source data.

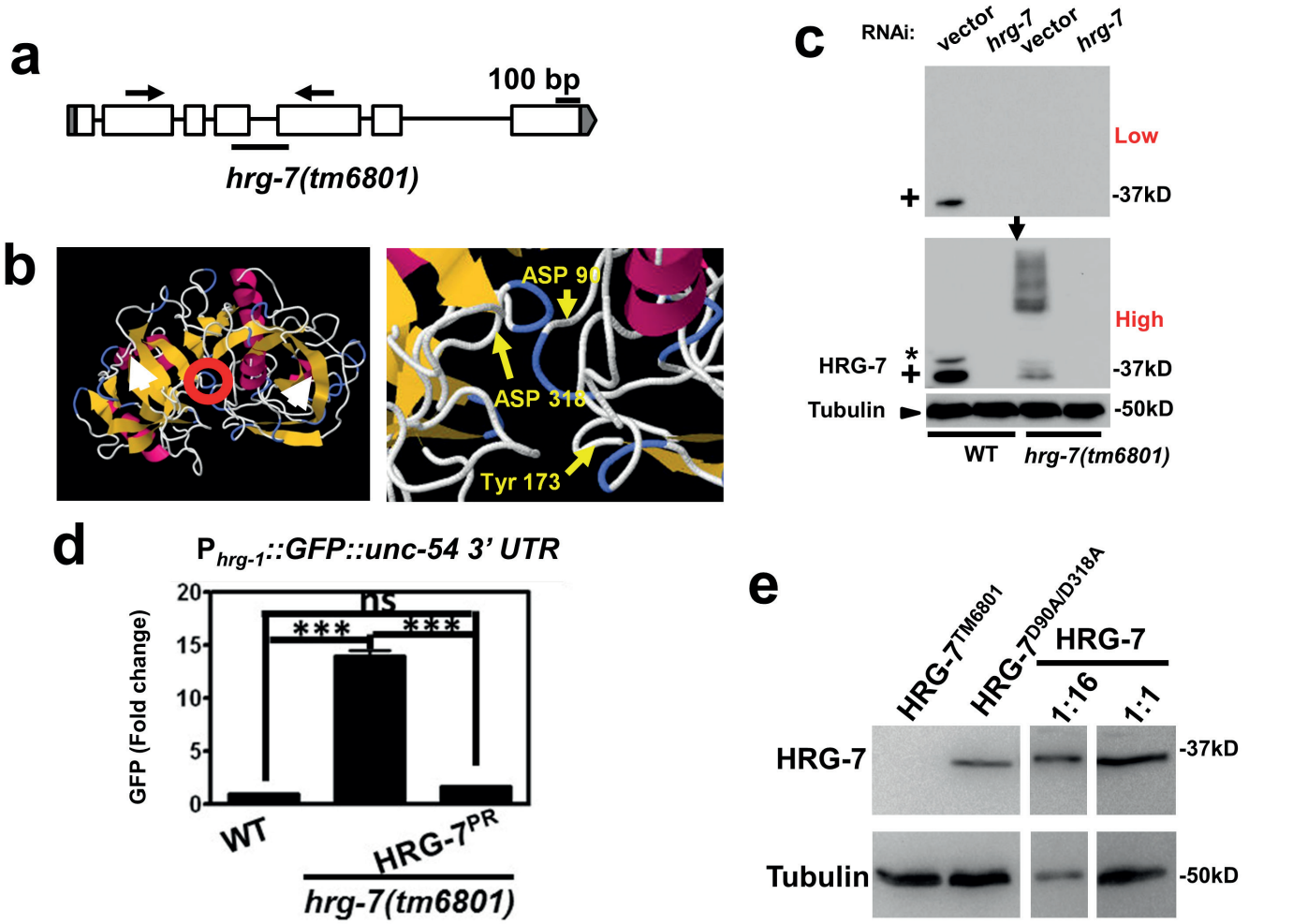

Supplementary Figure 4 Transgenic HRG-7 rescues *hrg-7* mutant phenotypes **a)** Cartoon depicting the deleted region of *hrg-7* in the *tm6801* allele. Deletion is depicted by an underline. Open rectangles, exons; gray boxes, untranslated regions. **b)** Homology model of HRG-7 using I-TASSER. Left: the putative active site is indicated by a red circle. The conserved disulfide bonds are indicated by white arrows. Alpha helixes are colored fuchsia. Beta sheets are colored yellow. Right: Zoomed in image of the putative active site. Yellow arrows indicate the catalytic aspartic acid residues and the conserved tyrosine of the flap region. **c)** Immunoblot analysis of HRG-7 expression in worms expressing WT HRG-7 or HRG-7^{TM6801} and fed dsRNA against control vector or hrg-7. Membranes were probed with polyclonal anti-HRG-7 antibody and then incubated with HRP-conjugated anti-rabbit secondary antibody. * indicates pro-HRG-7. + indicates mature HRG-7. "Low" indicates low sensitivity detection. "High" indicates high sensitivity detection. Unprocessed blots are shown in Figure S6. Data is representative of three independent experiments. **d)** GFP fluorescence quantified from IQ6011 expressing WT *hrg-7*, *hrg-7(tm6801)*, or *hrg-7(tm6801)* and transgenic P_{vha-6}*::hrg-*7^{PR} grown on OP50. GFP is presented as fold change compared to wild type (WT) worms. ***P<0.001, **P<0.01, *P<0.05 (one-way ANOVA). Graph represents the mean and SEM of three biological independent experiments. N=120 worms per treatment per experiment. See Supplementary Table 3 for statistics source data. **e)** Immunoblot analysis of titrated endogenous HRG-7 and HRG-7^{PR}*(D90A/D318A)* expressed in the *hrg-7(tm6801)* background. Membranes were probed with polyclonal anti-HRG-7 antibody and then incubated with HRP-conjugated anti-rabbit secondary antibody. Irrelevant lanes were removed from the image. Unprocessed blots are shown in Figure S6. Images are representative of two independent experiments.

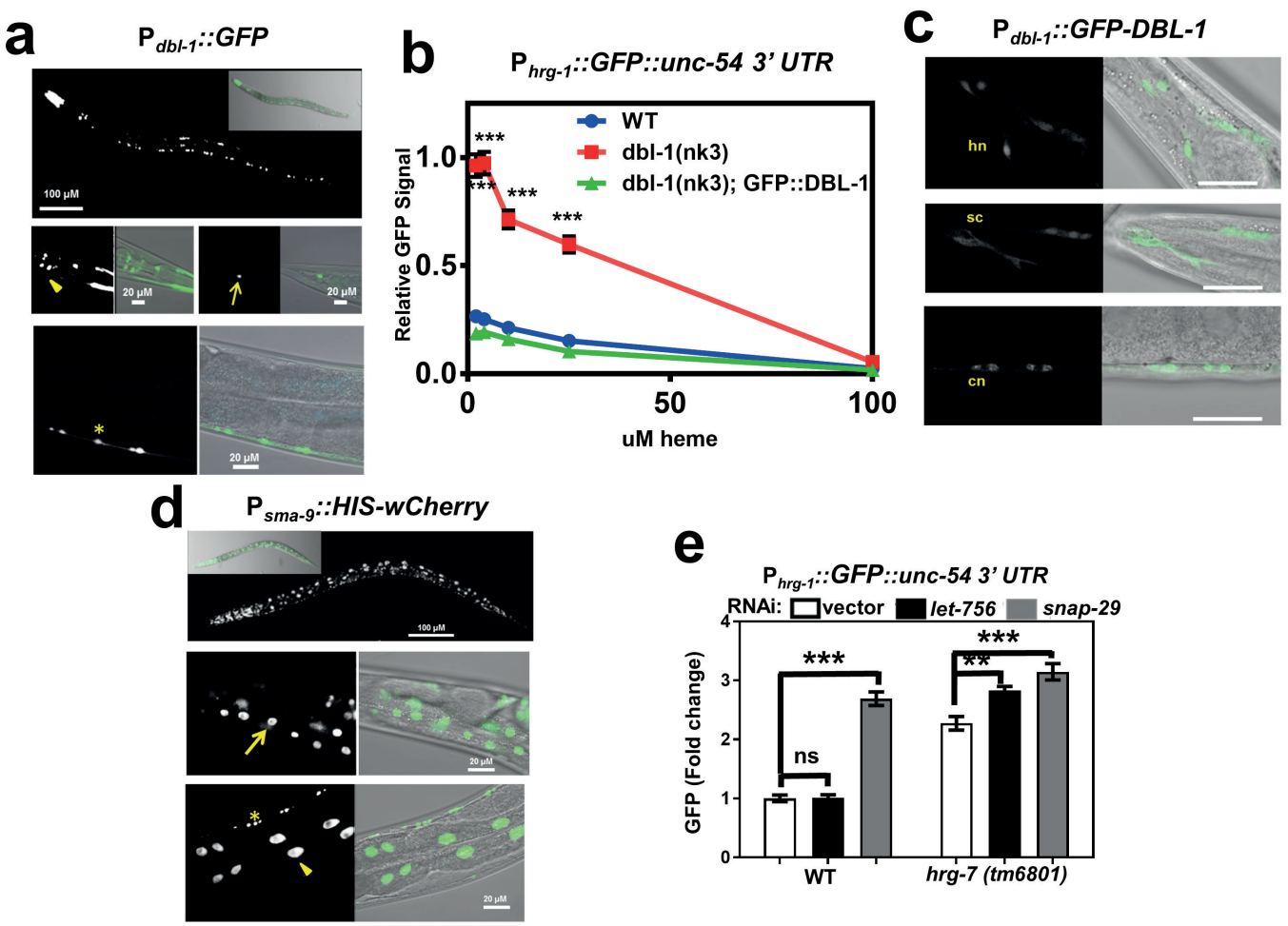

Supplementary Figure 5 Extra-intestinal regulation of intestinal *hrg-1*. **a)** GFP expression in strain BW1946 (*P*$_{dbl-1}$*::GFP*). Arrowhead indicates head neurons. Arrow indicates tail neurons. * indicates body neuron. Scale bar = 100 µm (top panel); Scale bar =20 µm (middle and lower panels). Images are representative of three independent experiments. **b)** GFP quantification from IQ6011, IQ6311, and IQ6312 grown on OP50 supplemented with indicated heme concentrations. GFP fluorescence was quantified using COPAS BioSort. GFP is presented as relative expression on a scale from 1-100. Graph represents the mean and SEM of 50 worms per strain per heme concentration combined from three biological independent experiments. ***P<0.001, **P<0.01, *P<0.05 compared to WT worms (two-way ANOVA). **c)** GFP-DBL-1 expression in strain VC1478. GFP signal was detected in neurons and neuron support cells. "hn" indicates head neuron. "sc" indicates support cells. "cn" indicates ventral nerve cord neuron. Scale bar = 20 µm. Images are representative of three independent experiments. **d)** wCherry expression in strain RW10745 (*P*$_{sma-9}$*::HIS-24-wCherry*). Arrow indicates hypodermal nuclei. Arrowhead and asterisks indicate intestinal and body neuron nuclei, respectively . Scale bar = 100 µm (top panel); Scale bar =20 µm (middle and lower panels). Images are representative of three independent experiments. **e)** GFP fluorescence quantified from IQ6011 expressing WT *hrg-7* or *hrg-7(tm6801)* and fed dsRNA against vector, *let-756*, or *snap-29*. GFP was quantified using COPAS BioSort. GFP is presented as fold change compared to vector. Graph represents the mean and SEM of 1000 worms per treatment combined from four biological independent experiments. ***P<0.001, **P<0.01, *P<0.05 (Dunnett's test).

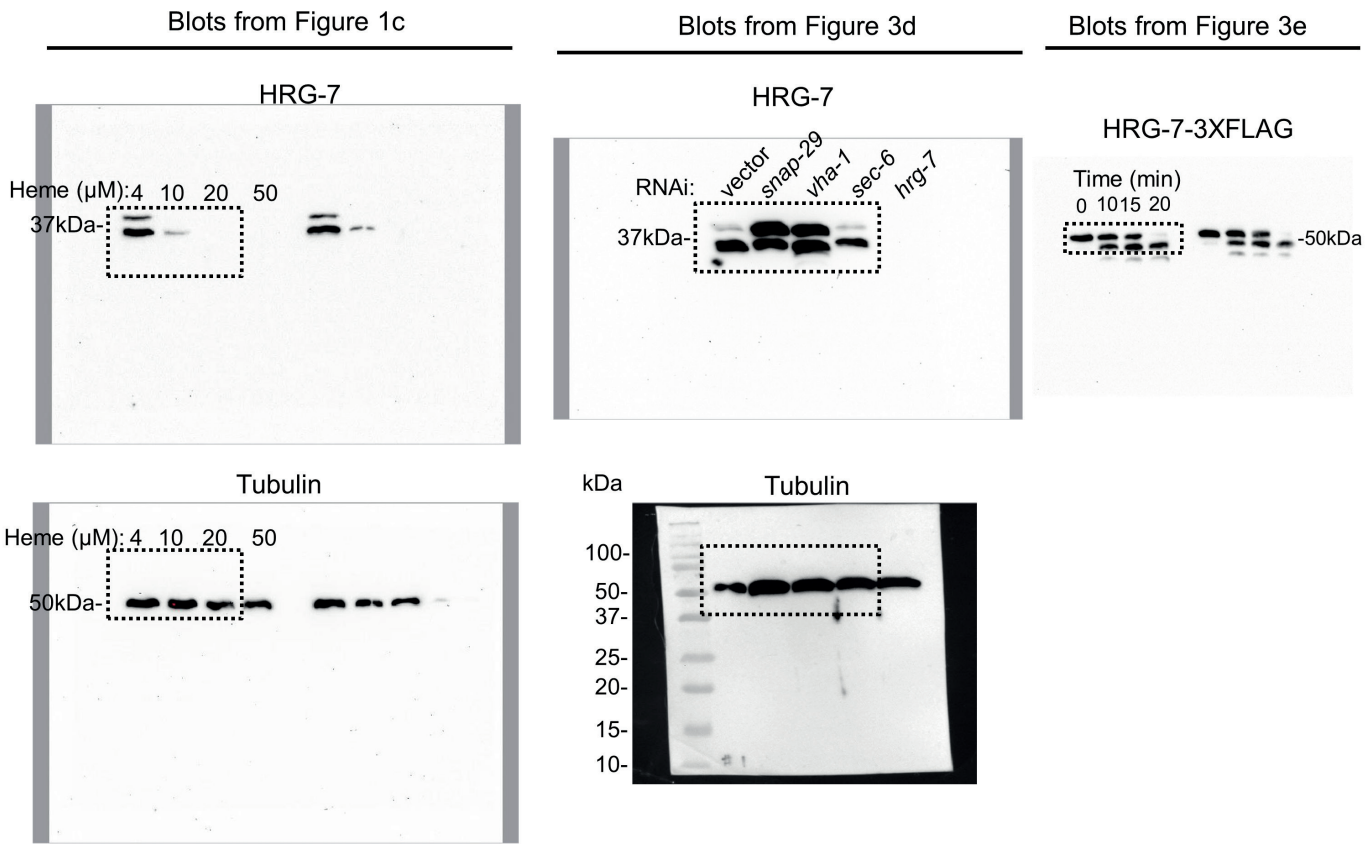

Supplementary Figure 6 Unprocessed western blot scans. Unprocessed western blots from Figures 1c, 3d, 3e, and Supplementary Figures 1e, 3c, 4c, 4e.

Supplementary Table legends

Supplementary Table 1 Related to Figure 3- Trafficking factors that regulate HRG-7::mCherry secretion**.** Full list of genes that result in aberrant HRG-7 secretion when depleted.

Supplementary Table 2 Related to Figure 5 -Secreted signaling factors knocked down by RNAi. Full list of signaling factors depleted by RNAi in IQ6015. GFP expression is shown as fold change compared to vector.

Supplementary Table 3 Statistics source data. Data from which statistics were derived for Figures 1a, 1e, 2f, 4c, 4d, 5b, 5e, 5f and Supplementary Figures 2a, 2f, 3d, 4d, 5e, 5f.

Supplementary Table 4 Regulators of *hrg-1*. Genes that result in regulation of $P_{hrg\text{-}1}$*::GFP* ≥ 2 fold (log scale) compared to $P_{vha\text{-}6}$*::GFP* when knocked down by RNAi.